Gas-filled spherical resonators: Theory and experiment

Michael R. Moldover
Thermophysics Division, National Bureau of Standards, Gaithersburg, Maryland 20899

James B. Mehl
Physics Department, University of Delaware, Newark, Delaware 19716

Martin Greenspan[a]
12 Granville Drive, Silver Spring, Maryland 20901

Gas-filled spherical resonators are excellent tools for routine measurement of thermophysical properties. The radially symmetric gas resonances are nondegenerate and have high Q's (typically 2000–10 000). Thus they can be used with very simple instrumentation to measure the speed of sound in a gas with an accuracy of 0.02%. We have made a detailed study of a prototype resonator filled with argon (0.1–1.0 MPa) at 300 K, with the objective of discovering those phenomena which must be understood to use gas-filled spherical resonators to measure the thermodynamic temperature and the universal gas constant R. The resonance frequencies f_N and half-widths g_N were measured for nine radially symmetric modes and nine triply-degenerate nonradial modes with a precision near $10^{-7}f_N$. The data were used to develop and test theoretical models for this geometrically simple oscillating system. The basic model treats the following phenomena exactly for the case of a geometrically perfect sphere: (1) the thermal boundary layer near the resonator wall, (2) the viscous boundary layer (for nonradial modes), (3) bulk dissipation, and (4) the coupling of shell motion and gas motion. In addition, the following phenomena are included in the model through the use of perturbation theory: (5) ducts through the shell, (6) imperfect resonator geometry, and (7) the seam where the two hemispheres comprising the shell are joined. Some estimates of the effects of (8) roughness of the interior of the shell have also been made. Much of the lower pressure f_N and g_N data can be explained by our model of these phenomena to within $\pm 5 \times 10^{-6} f_N$ when a single parameter $c_0/(V_0)^{1/3}$ is fit to a single resonance frequency at a single pressure. In this parameter, c_0 is the ideal-gas speed of sound and V_0 is the resonator volume. If this volume were known, the prototype resonator could be used to measure the speed of sound of a gas with an accuracy approaching $\pm 0.0005\%$. Improvements in resonator design which will circumvent difficulties discovered in this work are expected to lead to much better agreement between theory and the measured f_N and g_N.

PACS numbers: 43.20.Ks, 43.20.Rz, 43.85.Dj

LIST OF SYMBOLS

c	= speed of sound in gas
c_{sh}	= speed of longitudinal waves in shell materials
C_p, C_v	= specific heats per unit mass
D_v	= η/ρ = coefficient of viscous diffusivity
D_t	= $K/(\rho C_p)$ = coefficient of thermal diffusivity
f	= $\omega/(2\pi)$ = frequency
F_N	= $F_{nsm} = f_N + ig_n$ = complex resonance frequency
$j_n(z)$	= nth-order spherical Bessel function
k	= ω/c
k_{sh}	= ω/c_{sh}
K	= thermal conductivity
$\mathbf{n}_r$	= unit vector in radial direction
p	= acoustic pressure
P	= absolute pressure
S	= entropy per unit mass
T	= absolute temperature

$\mathbf{u}$	= acoustic particle velocity in fluid
$Y_{nm}(\theta,\phi)$	= spherical harmonic
	$\propto P_n^m(\theta)\cos m\phi, \quad m \geqslant 0$
	$\propto P_n^{-m}(\theta)\sin m\phi, \quad m < 0$
z_{ns}	= s th solution of $dj_n(z)/dz = 0$
α	= $(\partial P/\partial T)_v$
$\beta(\omega,r)$	= specific acoustic admittance
γ	= C_p/C_v = specific heat ratio
δ_v	= $\sqrt{2D_v/\omega}$ = viscous boundary layer thickness
δ_t	= $\sqrt{2D_t/\omega}$ = thermal boundary layer thickness
δ_v'	= $\sqrt{\frac{4}{3}\delta_v^2 + \eta_b/\rho}$
η, η_b	= shear, bulk viscosity coefficients
λ, μ	= Lamé constants
ρ	= gas density
ρ_{sh}	= shell density
σ	= Poisson's ratio
τ	= acoustic temperature

---

[a] National Bureau of Standards, retired.

INTRODUCTION

Gas-filled spherical resonators comprise mechanical systems whose properties are easy to model with extraordinary accuracy. Thus they are now being used for a measurement of the universal gas constant R, where an accuracy approaching a few parts in 10^6 is expected.[1] This measurement provides a motivation for understanding the resonance frequencies to an accuracy of one part in 10^6. Other applications are less demanding. These applications include "routine" accurate measurements of the speed of sound in gases, particularly at low reduced temperatures where other methods of measurement of virial coefficients fail.[2-5] Spherical resonators have also been used for monitoring the composition of binary gas mixtures.[6,7] They are being developed for acoustic thermometry[1] and have applications to photoacoustic spectroscopy.[8] Spherical resonators can be used as enclosures for calibration of microphones via reciprocity and it is plausible that spherical resonators can be used for the measurement of the thermal conductivity of gases.

The intent of this article is to provide a self-contained summary of our understanding of and experience with spherical resonators. This Introduction will be followed by a formal presentation of our theoretical model of the spherical resonator. The formal theory includes an exact solution of the "three-mode" problem for a spherical resonator. That is, the coupling of the pressure field, the temperature field, and the shear velocity field is formulated exactly, and a boundary condition which includes all viscous and thermal effects as well as the effects of nonzero shell admittance is derived. The theory of the shell admittance includes the effects of radiation from the outer surface of the shell and internal losses within the shell. While the focus of the theory section is on applications to gas-filled resonators, most of the results are applicable to liquid-filled resonators.

The major results of the formal theory are referenced in later sections for the benefit of the reader who prefers a more descriptive approach. The next major section is a description of our prototype resonator. This is followed by a short discussion of the dominant physical phenomena required to model gas-filled spherical resonators in the regime where they are most frequently applied. We then proceed to a description of a representative set of experiments which illustrate these phenomena. In the concluding section, some further improvements are suggested.

The significant practical advantages of spherical resonators apply to the radially symmetric gas resonances. These resonances have exceptionally high Q's (see Ref. 9) and they are nondegenerate. For these modes, the gas motion is perpendicular to the inside surface of the resonator's shell; thus the motion is not subject to viscous damping at the gas–shell boundary. When our 1-liter resonator is filled with argon (or air) at ambient temperature and at pressures in the range 0.1–1.0 MPa, the lowest five radial resonances have Q's ranging from 2000–10 000. The high Q's of the radially symmetric modes permit the use of small, inefficient transducers embedded in the resonator's shell which perturb the resonator geometry in a minor and predictable way.

The nondegenerate nature of the radially symmetric modes is significant for two reasons. First, one can show that

the resonance frequencies are insensitive to geometrical imperfections in the first order of perturbation theory. Thus a resonator which has been constructed with ordinary machine-shop tolerance can be used for extremely accurate speed of sound measurements without making any dimensional measurements other than the volume of the resonator. (The volume itself can be easily obtained with high accuracy from measurements of resonance frequencies when the resonator is filled with a reference gas such as argon.) Second, measurements of the resonance widths of these nondegenerate modes can be interpreted directly in terms of the properties of the gas. When degeneracies are present, the apparent width of unresolved or partially resolved modes depends upon details of the resonator's geometry and the transducer's properties as well as the gas' properties.

The symmetry of the spherical resonator facilitates detailed analytic calculations of the pertubations to the resonance frequencies from physical phenomena which can be described by an acoustic admittance at the gas–shell boundary. The most important of these are (1) the thermal boundary layer near the resonator wall, (2) the viscous boundary layer (for nonradial modes), and (3) finite elastic compliance of the resonator shell. We shall also mention the smaller perturbations to the resonance frequencies resulting from holes drilled in the shell, including a vent hole and a duct leading from the interior to a transducer, imperfect resonator geometry, the seam where the two hemispheres comprising the shell are joined, and finally roughness of the interior of the shell (such as that left from machining).

At the pressures of interest here (0.1–1.0 MPa), dissipation in the gas resulting from thermal conductivity and viscosity (and relaxation in polyatomic gases) is important. The ratio of the acoustic pressure to the static pressure is always less than 10^{-6}; thus nonlinear effects are not important. At the lowest pressures and highest frequencies discussed here, the ratio of the mean free path to the wavelength of sound becomes as large as 5×10^{-6}. Nevertheless, corrections to hydrodynamics remain quite small.[10] (The effects of incomplete thermal accommodation of the gas with a spherical shell have been observed[5,11] at lower pressures near 10 kPa.)

Very large perturbations occur when a resonator is filled with a gas under conditions approaching condensation. These were recently discussed in detail elsewhere.[12]

One can show that, under most conditions, the acoustic radiation from the exterior surface of a gas-filled resonator, either through a gas or through supports, is negligible.

Our theory of spherical resonators will be tested by measurements of the frequencies and half-widths of nine radial and nine nonradial (triply-degenerate) modes when our 1-liter aluminum resonator is filled with argon at seven pressures spanning the range 0.1–1.0 MPa and at a temperature near 296.31 K. Under these conditions, most of the auxiliary quantities needed to test the theory (thermal conductivity, viscosity, and first acoustic virial coefficient A_1) are well known from independent measurements. The measurements have a frequency resolution exceeding 1 part in 10^6. If our understanding were complete and if our measurements were free of systematic error, all 252 frequencies and 252

half-widths would be fitted by two parameters: $c_0/(V_0)^{1/3}$ and A_2. (Here, V_0 is the volume of the resonator at 296.31 K and zero pressure, c_0 is the speed of sound in argon at 296.31 K and zero pressure, and A_2 is the second acoustic virial coefficient of argon at 296.31 K.) For five of the radially symmetric modes, this appears to be true at the level of 10 parts in 10^6. The evidence we present suggests that it will be possible to construct new resonators for which theory and experiment agree near the level of 1 part in 10^6.

I. ACOUSTICAL MODEL FOR THE SPHERICAL RESONATOR

In this section, we describe the acoustical model of the spherical resonator. The model includes a calculation of the response of the gas and the shell to excitation by a steady sinusoidal stimulus, and also includes calculation of the fundamental resonance parameters which appear in the response function. It is convenient to assume that all of the "small" quantities of linear acoustics are proportional to $e^{i\omega t}$, and to obtain solutions in the form of linear combinations of appropriate eigenfunctions. In the following development, we assume the eventual inclusion of a source term whose strength and frequency remain constant long enough for the system to reach a steady state.

Let the acoustic field be described by a velocity potential $\Psi(\mathbf{r})$. In the lowest order of approximation, with all dissipative effects neglected, the acoustic pressure and particle velocity are related to $\Psi(\mathbf{r})$ by

$$p(\mathbf{r}) = -i\omega\rho\Psi(\mathbf{r}) \tag{1}$$

and

$$\mathbf{u}(\mathbf{r}) = \nabla\Psi(\mathbf{r}), \tag{2}$$

where $\Psi(\mathbf{r})$ is a solution of

$$(\nabla^2 + \omega^2/c^2)\,\Psi(\mathbf{r}) = 0. \tag{3}$$

The boundary condition can be conveniently stated in terms of a specific acoustic admittance

$$\frac{\partial\Psi(\mathbf{r})}{\partial n} = -i\left(\frac{\omega}{c}\right)\beta(\omega,\mathbf{r}_s)\,\Psi(\mathbf{r}), \tag{4}$$

where $\beta(\omega,\mathbf{r}_s)$ is defined to be the normal component of $\rho c \mathbf{u}/p$ at position $\mathbf{r}_s$ on the boundary. It is convenient to seek solutions of Eq. (3) in the form of linear combinations of eigenfunctions satisfying

$$(\nabla^2 + k_N^2)\,\Psi_N(\mathbf{r}) = 0 \tag{5}$$

and the boundary condition (4). The effects of geometric imperfections will be considered later in this section. For an ideal spherical geometry, the eigenfunctions are

$$\Psi_{nsm}(\mathbf{r}) \propto j_n(k_{ns}r)Y_{nm}(\theta,\phi), \tag{6}$$

where the k_{ns} are determined by the boundary condition at $r = a$. For the case where β is independent of position, the boundary condition is

$$kaj_n'(ka) = -i\,(\omega a/c)\,\beta(\omega)\,j_n(ka), \tag{7}$$

which can always be solved numerically for the $k_{ns}a$. In the limiting case of a uniform, rigid, fixed shell with perfectly insulating walls, the specific admittance is zero, and the

eigenvalues are the roots of $j_n'(z) = 0$. Let z_{ns} be the s th such root. There are $2n + 1$ degenerate modes with the indices (ns); the frequency of these modes in this zero-order approximation is $cz_{ns}/(2\pi a)$.

In the following sections we develop more accurate expressions for the frequencies of the modes. The major effects come from viscous and thermal effects at the shell boundary, and the finite acoustic impedance of the shell. These boundary effects, along with bulk viscous and thermal effects, are treated in the next section on wave modes. These effects, along with the smaller effects due to the fill duct and transducer coupling duct, shift the frequencies of the modes from the ideal values $cz_{ns}/(2\pi a)$. It is convenient to represent the frequencies in the complex form $F_N = f_N + ig_N$, where the imaginary term describes either the decay of free oscillations or the resonance half-width in steady-state measurements.

A. Wave modes

We begin our analysis of the wave modes of an acoustic resonator with the equations derived by Kirchhoff in 1868.[13,14] We assume a spherical coordinate system with the origin at the center of a geometrically perfect shell.

Kirchhoff assumed that the pressure, temperature, and particle velocity were described by the Navier–Stokes equation, the equations of continuity of mass and entropy, and Fourier's law of heat flow. Let the pressure and temperature be represented by $P + p(\mathbf{r})$ and $T + \tau(\mathbf{r})$, where P and T are the ambient quantities, and $p(\mathbf{r})$ and $\tau(\mathbf{r})$ are small terms with the assumed time dependence. The equations of motion couple these fields with each other and with the longitudinal particle velocity $\mathbf{u}(\mathbf{r})$. Kirchhoff found that $\tau(\mathbf{r})$ was governed by a fourth-order partial differential equation. It is convenient to write this equation in the form

$$(i\delta_t^2/2)\,[1 + (i\gamma/2)\,(\omega\delta_v'/c)^2]\nabla^4\tau$$
$$+ [1 + (i/2)\,(\omega/c)^2(\gamma\delta_t^2 + \delta_v'^2)]\,\nabla^2\tau$$
$$+ (\omega/c)^2\tau = 0. \tag{8}$$

The characteristic lengths in this equation are the thermal penetration length

$$\delta_t = \sqrt{2D_t/\omega}, \tag{9}$$

and a quantity δ_v', which is related to the viscous penetration length

$$\delta_v = \sqrt{2D_v/\omega}, \tag{10}$$

and the bulk viscosity η_b, by

$$\delta_v'^2 = \tfrac{4}{3}\delta_v^2 + \eta_b/\rho. \tag{11}$$

For argon at 300 K and 0.1 MPa, with a frequency of 10 □, approximate values for these lengths are $\delta_t = 21\,\mu\text{m}$, $\delta_v = 26\,\mu\text{m}$, and $\delta_v' = 30\,\mu\text{m}$. (For argon and other monatomic gases, the bulk viscosity term is negligible; it is included in the formalism for completeness.) Following Kirchhoff, we proceed by obtaining solutions for $\tau(\mathbf{r})$. From these we determine the pressure and particle velocity. Morse and Ingard[15] show that the pressure is related to the temperature through

$$p(\mathbf{r}) = [\gamma a/(\gamma - 1)]\,[1 - (\delta_t^2/2i)\,\nabla^2]\,\tau(\mathbf{r}), \tag{12}$$

and that the longitudinal particle velocity $u(r)$ is given by

$$i\omega \rho \mathbf{u} = - \boldsymbol{\nabla} \left[p + (i\gamma/2) (\omega \delta_v'/c)^2 (p - \alpha\tau) \right]. \quad (13)$$

[The derivation of Morse and Ingard makes it clear that Eqs. (8), (12), and (13) apply to dense fluids as well as to gases.] Equation (13) does not represent the complete gas velocity. A divergence-free component $\mathbf{w}(r)$, a solution of the transverse part of the Navier–Stokes equation

$$i\omega \rho \mathbf{w}(\mathbf{r}) = \eta \nabla^2 \mathbf{w}(\mathbf{r}), \quad (14)$$

can be added to u. Solutions of Eq. (14) will be needed later to satisfy boundary conditions at the resonator wall.

Equation (8) separates into

$$(\nabla^2 + k_p^2)(\nabla^2 + k_t^2) \tau (\mathbf{r}) = 0, \quad (15)$$

where k_p^2 and k_t^2 are the roots of a bi-quadratic equation whose coefficients can be determined from Eq. (8). It is most convenient to write expressions for these roots in the form of series expansions of the exact solutions:

$$k_p^2 = \left(\frac{\omega}{c}\right)^2 \left[1 - \left(\frac{i}{2}\right) \left(\frac{\omega}{c}\right)^2 [(\gamma - 1) \delta_t^2 + \delta_v'^2] \right.$$
$$\left. + O\left(\frac{\omega\delta}{c}\right)^4 \right], \quad (16)$$

$$k_t^2 = \left(\frac{-2i}{\delta_t^2}\right) \left[1 + \left(\frac{i}{2}\right) \left(\frac{\omega}{c}\right)^2 (\gamma - 1) (\delta_t^2 - \delta_v'^2) \right.$$
$$\left. + O\left(\frac{\omega\delta}{c}\right)^4 \right]. \quad (17)$$

The notation here indicates that the solutions are correct to fourth order in the ratio of any of the characteristic lengths δ to the wavelength of an acoustic wave.

Kirchhoff found solutions of Eq. (8) for plane waves and spherical outgoing waves in an unbounded medium, and for waves propagating along the axis of a circular tube. It is also possible to write down exact solutions for standing waves in a spherical geometry. Solutions which are finite at the origin have the form

$$\tau (\mathbf{r}) = [\tau_p j_n (k_p r) + \tau_t j_n (k_t r)] Y_{nm} (\theta, \phi). \quad (18)$$

From Eq. (17) we see that k_t is approximately equal to $(1 - i)/\delta_t$. Thus the term $j_n (k_t r)$ varies rapidly with r. For large values of r/δ_t, the asymptotic form $j_n (z) \approx \cos[z + (n + 1)\pi/2]/z$ can be used. With $z = k_t r$, the amplitude of this expression is approximately $\exp(r/\delta_t)/(r/\delta_t)$, which decays rapidly with decreasing r. Thus the behavior of the exact solution (18) is similar to the behavior of the approximate boundary layer solutions presented in many texts. The contribution of Eq. (18) proportional to τ_t is only important within a few boundary layer thicknesses δ_t of the wall.

The pressure corresponding to Eq. (18) is

$$p(\mathbf{r}) = \frac{\gamma\alpha}{\gamma - 1} \left[\tau_p \left(1 + \frac{\delta_t^2 k_p^2}{2i} \right) j_n (k_p r) \right.$$
$$\left. + \tau_t \left(1 + \frac{\delta_t^2 k_t^2}{2i} \right) j_n (k_t r) \right] Y_{nm}. \quad (19)$$

The longitudinal particle velocity is given by

$$\rho c \mathbf{u}(\mathbf{r}) = \frac{ic}{\omega} \frac{\gamma\alpha}{\gamma - 1} \boldsymbol{\nabla} \left[F(k_p^2) \tau_p j_n (k_p r) Y_{nm} \right.$$
$$\left. + F(k_t^2) \tau_t j_n (k_t r) Y_{nm} \right], \quad (20)$$

where

$$F(k^2) \equiv 1 + \left(\frac{i}{2}\right) \left(\frac{\omega\delta_v'}{c}\right)^2 - \left(\frac{i}{2}\right)(k\delta_t)^2$$
$$+ \left(\frac{\gamma}{4}\right) \left(\frac{\omega\delta_v'\delta_t k}{c}\right)^2. \quad (21)$$

We also need an expression for the transverse velocity field. Equation (14) can be written

$$(\nabla^2 + k_v^2) \mathbf{w} (\mathbf{r}) = 0, \quad (22)$$

where

$$k_v^2 = \eta/(i\omega\rho) = -2i/\delta_v^2. \quad (23)$$

The general solution of the vector Helmholtz equation (22) is a superposition of a longitudinal field and two transverse fields. Only the latter are admissible here. The solution has the form[16]

$$\mathbf{w}(\mathbf{r}) = W_1 \boldsymbol{\nabla} \times [\mathbf{n}_r r j_n (k_v r) Y_{nm}]$$
$$+ (W_2/k_v) \boldsymbol{\nabla} \times \boldsymbol{\nabla} \times [\mathbf{n}_r r j_n (k_v r) Y_{nm}], \quad (24)$$

where W_1 and W_2 are constant parameters and $\mathbf{n}_r$ is a unit vector in the radial direction. Like the thermal contribution in Eq. (18), the shear wave solution is significant only within a few boundary layers δ_v of the wall.

B. Boundary conditions

We now have the formalism necessary to satisfy appropriate boundary conditions at the shell wall. We require that (1) the temperature and heat current are continuous at the wall, (2) the tangential components of the total velocity $u + v$ vanish at the wall, and (3) the ratio of the normal component of the velocity to the pressure is equal to an effective acoustic admittance.

Herzfeld[17] showed that when the product of the thermal conductivity and specific heat per unit volume of the shell material greatly exceeds the corresponding quantity of the gas, the first condition is practically equivalent to the requirement that the temperature be constant on the shell wall. For a typical gas in a metal shell the temperature amplitude at the gas–shell interface is on the order of 10^{-4} of the temperature amplitude well within the gas. It is thus an excellent approximation to simply require that $\tau(\mathbf{r})$ vanish for $r = a$, which fixes the ratio of the constants in Eq. (18) through

$$\tau_p j_n (k_p a) + \tau_t j_n (k_t a) = 0. \quad (25)$$

The constants W_1 and W_2 in Eq. (24) are determined by the condition that the θ and ϕ components of $u + w$ equal the corresponding components of the shell velocity. The latter are zero in the approximation that the shell is infinitely rigid, and are small under the conditions of our experiment. Their inclusion in the theory leads to a small correction to a term which is itself a small correction. We thus assume for simplicity, without significant loss of accuracy, that the θ and ϕ

components of $u + w$ vanish at $r = a$. The two conditions are actually equivalent, and are satisfied if $W_1 = 0$ and if W_2 is given by

$$W_2 = \frac{\gamma\alpha}{i\omega\rho a(\gamma - 1)}$$

$$\times \frac{F(k_p^2)\,\tau_p\,j_n(k_p a) + F(k_t^2)\,\tau_t\,j_n(k_t a)}{j_n'(k_v a) + j_n(k_v a)/(k_v a)}. \quad (26)$$

The transverse velocity has a radial component

$$w_r\,(r,\theta,\phi) = W_2[\,j_n(k_v r)/(k_v r)\,]n(n+1)\,Y_{nm}\,(\theta,\phi), \quad (27)$$

which contributes to the remaining boundary condition at $r = a$:

$$\rho c\,(u_r + w_r) = \beta_{\mathrm{sh}}\,(\omega)\left(p - \frac{4}{3}\eta\,\frac{\partial u_r}{\partial r}\right). \quad (28)$$

Here $\beta_{\mathrm{sh}}\,(\omega)$ is the specific acoustic admittance for the shell. For a given shell this quantity is a calculable function of the frequency and mode index n. It is discussed further in the following section. The right side of Eq. (28) is the product of β_{sh} and the negative of the stress in the fluid. The latter differs from the acoustic pressure by a factor of $1 + O\,(\omega\delta/c)^2$. For simplicity, we neglect this small correction. From Eqs. (19), (20), and (25)–(28), we then obtain

$$\frac{2c}{\omega a\delta_t^2}\frac{1}{k_t^2 - k_p^2}\left(F(k_p^2)\frac{k_p a\,j_n'(k_p a)}{j_n(k_p a)}\right.$$

$$- F(k_t^2)\frac{k_t a\,j_n'(k_t a)}{j_n(k_t a)} - [F(k_p^2) - F(k_t^2)]$$

$$\left.\times\frac{n(n+1)}{1 + k_v a\,j_n'(k_v a)/j_n(k_v a)}\right) = \beta_{\mathrm{sh}}\,(\omega). \quad (29)$$

Except for a small correction to the right-hand side, this equation is exact. The next step is to eliminate k_p^2, k_t^2, and k_v^2. This, along with an expression for the shell admittance, leads to an equation which determines the complex resonance frequencies of the gas in the shell. In principle, the exact expression for k_p^2, k_t^2, and k_v^2 could be used in determination of the resonance frequencies. We can obtain sufficient accuracy by using the series expansions (16) and (17) of the exact solutions. These lead to the following expressions for the functions $F(k^2)$:

$$F(k_p^2) = 1 + (i/2)\,(\omega/c)^2(\delta_v'^2 - \delta_v^2) + O(\omega\delta/c)^4, \quad (30)$$

$$F(k_t^2) = (-i/2)\,(\omega\delta_t/c)^2(\gamma - 1) + O(\omega\delta/c)^4. \quad (31)$$

To lowest order, k_t is equal to $(1 - i)/\delta_t$. Thus the magnitude of $k_t a$ is of order a/δ_t, and the asymptotic form can be used for the spherical Bessel functions in Eq. (29):

$$j_n'(k_t a)/j_n(k_t a) \approx -\tan[k_t a - (n+1)\,\pi/2]$$

$$\approx i + O\,(e^{-2a/\delta_t}). \quad (32)$$

Similarly, since k_v is exactly $(1 - i)/\delta_v$, the expression $1 + k_v a\,j_n'(k_v a)/j_n(k_v a)$ in Eq. (29) can be approximated by $ik_v a$. With these approximations, Eq. (29) becomes

$$-i\left(\frac{\omega a}{c}\right)\beta_{\mathrm{sh}} = \frac{k_p a\,j_n'(k_p a)}{j_n(k_p a)} - \frac{1 - i}{2}$$

$$\times\left((\gamma - 1)\frac{\omega^2 a^2}{c^2}\frac{\delta_t}{a} - n\,(n+1)\frac{\delta_v}{a}\right), \quad (33)$$

where the right-hand side of this is correct to within a multiplier $1 + O\,(\omega\delta/c)^2$. Equation (33) can be rearranged as

$$k_p a\,j_n'(k_p a)/j_n(k_p a) = -i\,(\omega a/c)\,(\beta_{\mathrm{sh}} + \beta_t + \beta_v), \quad (34)$$

where

$$\beta_t = \tfrac{1}{2}\,(1 + i)\,(\omega/c)\,(\gamma - 1)\,\delta_t \quad (35)$$

is the thermal contribution to the acoustic admittance and

$$\beta_v = \tfrac{1}{2}\,(1 + i)\,(c/\omega)\,n\,(n+1)\,\delta_v/a^2 \quad (36)$$

is the viscous contribution to the acoustic admittance.

Equation (34) is an approximation to the more accurate boundary condition (29), and has the same form as Eq. (7). We thus see that the thermal and viscous effects can be included in Eq. (7) to order $(\omega\delta/c)^2$ by introduction of the boundary admittances given by Eqs. (35) and (36), and use of Eq. (16) to relate k_p to the frequency.

Equation (34) can always be solved numerically for the quantities $k_p a$. These can then be related to complex resonance frequencies $F_N = f_N + ig_N$ through Eq. (16). Note that the thermal and viscous terms are generally small for both gases and liquids, but the shell admittance is not necessarily small. Thus it is worth developing approximate solutions for this case. Let $k_0 a = \omega_0 a/c$ be any solution of

$$j_n'(k_0 a)/j_n(k_0 a) = -i\beta_{\mathrm{sh}}. \quad (37)$$

Now, the relation between k_p and ω in Eq. (16) can be expressed to order $(\omega\delta/c)^4$ as

$$k_p a = (a/c)\,(\omega_0 + \Delta\omega - 2\pi i g_{\mathrm{bulk}}) = k_0 a + \Delta ka, \quad (38)$$

where

$$g_{\mathrm{bulk}} = \frac{\pi^2 f^3}{c^2}\left((\gamma - 1)\,\delta_t^2 + \frac{4}{3}\delta_v^2 + \frac{\eta_b}{\rho\,\omega}\right) \quad (39)$$

can be identified as the contribution to the imaginary part of the resonance frequency which is proportional to the bulk attenuation of sound. In small terms like (39), f represents either the source frequency in steady-state measurements or the real part of the mode frequency in free decay.

We next approximate $j_n\,(k_p a)$ and $j_n'(k_p a)$ in Eq. (35) as follows:

$$j_n(k_p a) = j_n(k_0 a) + j_n'(k_0 a)\,\Delta ka + O\,(\Delta ka)^2,$$

$$j_n'(k_p a) = j_n'(k_0 a) + j_n''(k_0 a)\,\Delta ka + O\,(\Delta ka)^2, \quad (40)$$

$$j_n''(k_0 a) = -\frac{2}{k_0 a}j_n'(k_0 a) + \left(1 - \frac{n\,(n+1)}{(k_0 a)^2}\right)j_n(k_0 a).$$

The last of these, the differential equation for $j_n\,(z)$, can be used to eliminate the second derivative $j_n''(k_0 a)$. The remaining spherical Bessel function terms involve only the ratio on the left side of Eq. (37), and can be expressed in terms of β_{sh}. The result, correct to order $(\Delta ka)^2$, is

$$\frac{\Delta\ (ka)}{k_0 a} = \frac{\Delta f + ig - ig_{bulk}}{f}$$

$$= \frac{-i\ (\beta_t + \beta_v)/(k_0 a)}{[1 - n\ (n+1)/(k_0 a)^2] + i\beta_{sh} - \beta_{sh}^2}. \quad (41)$$

Two limiting cases are of interest. For an infinitely rigid shell, the shell admittance β_{sh} vanishes, and the solutions $k_0 a$ of Eq. (37) are the z_{ns} and Eq. (41) is

$$\frac{\Delta F_{ns}}{f} = \frac{ig_{bulk}}{f} - \frac{i\ (\beta_t + \beta_v)/z_{ns}}{1 - n\ (n+1)/z_{ns}^2}$$

$$= \frac{ig_{bulk}}{f} - \frac{1 - i}{2a}\frac{(\gamma - 1)\ \delta_t + n\ (n+1)\ \delta_v/z_{ns}^2}{1 - n\ (n+1)/z_{ns}^2}. \quad (42)$$

Equation (42) shows that the thermal and viscous boundary effects each contribute to the shifts to the real and imaginary parts of the resonance frequency, and that the magnitudes of the real and imaginary contributions are equal. Equation (42) also shows that the bulk thermal and viscous effects only contribute to the imaginary part of the resonance frequency.

For gases in a metal shell, it is nearly always a good approximation to assume that the shell admittance is small. The exception is when an acoustic resonance frequency and a shell resonance frequency nearly coincide. In such cases, magnitude of the shell admittance can be very large. The specific acoustic admittance of the shell, as defined in Eq. (28), is directly proportional to the gas density. Thus, for very high density gases or liquids, the magnitude of the shell admittance can be large over a wide range of frequencies, particularly for the relatively thin resonators often used in studies of liquids. The solutions of Eq. (35) for the case $|\beta_{sh}| > 1$ correspond to the "pressure release" boundary condition, i.e., they are close to the roots of the spherical Bessel function rather than its derivative. For these cases, Eq. (41) shows that the thermal and viscous boundary effects vanish. The reason can be seen in Eqs. (25) and (26), which show that τ_t, the magnitude of the thermal wave, and W_2, the amplitude of the transverse wave, are both proportional to $j_n\ (k_p a)$, which vanishes when $|\beta_{sh}|$ is infinite.

Formally, Eq. (20) gives an expression for the velocity potential Ψ_N in Eq. (2). This velocity potential can still be associated with the mode indices $N = (nsm)$, but is no longer a solution of Eq. (3) with the simple form given in Eq. (6). The differences, however, are of order $(\omega\delta/c)^2$. To lowest order the relation between Ψ_N and p expressed in Eq. (19) is equivalent to that given in Eqs. (1)–(2). For calculation of the measured resonator response and calculation of certain higher-order effects, the differences between the zero-order description given by Eqs. (1)–(6) and the more accurate description developed in this and the previous section can be neglected. The main thermal and viscous effects are the effects on the resonance frequencies, which are represented with sufficient accuracy by, e.g., Eq. (41).

Some preliminary modeling calculations have been carried out to determine the effect of lack of smoothness of the surface finish on the thermal boundary layer perturbation. For these calculations, the surface was assumed to have a sinusoidal profile of amplitude $\delta \ll \delta_t$. (Such a finish might be left by machine tools.) The results seem to be sensitive mainly to the parameter δ and not to the horizontal spacing of the surface undulations (over a reasonable range of parameters). The calculations suggest that Δf_t is increased by a factor $(1 + 2\delta/\delta_t)$ and that Δg_t is not affected. [Here Δf_t and Δg_t refer to the thermal contribution to Eq. (42).]

C. Shell motion

The theory of the interaction of a uniform spherical shell with an internal acoustic mode was first worked out by Greenspan for the purely radial case.[18] Mehl recently treated the general nonradial case.[19] In this section, we present a brief treatment of the radial case. We include the effects of radiation from the outer surface of the shell and of internal dissipation in the shell. The objective is to calculate the effective acoustic admittance of the shell $\beta_{sh}\ (\omega)$, which was referred to in the previous sections. We also summarize the results for the $n = 1$ nonradial case. Modes with $n > 1$ were not studied in the present work.

We assume a uniform spherical shell with inner radius a and outer radius b. We assume that the shell is surrounded by a fluid which is not necessarily the same as the fluid enclosed in the shell. Thus this calculation could apply, for example, to a liquid-filled resonator which is surrounded by air. We neglect the coupling to the outside world through the mechanical supports.

We assume that the shell material is isotropic with Lamé constants λ and μ. The speed of longitudinal waves in the shell is

$$c_{sh} = \sqrt{(\lambda + \mu)/\rho_{sh}}. \quad (43)$$

For the radially symmetric case, the displacement in the radial direction $s_r\ (r)$ is the derivative of a scalar solution of the Helmholtz equation, which we write as

$$s_r = \frac{\partial H_0(k_{sh}r)}{\partial r}, \quad (44)$$

where $k_{sh} = \omega/c_{sh}$ and

$$H_n\ (z) = a_1 j_n\ (z) + a_2 y_n\ (z) \quad (45)$$

is a linear combination of spherical Bessel and Neumann functions. The boundary condition at $r = a$ requires that the normal stress in the gas, which we approximate by the negative acoustic pressure [refer to the discussion following Eq. (28)], be the negative of the rr component of the stress tensor, and that the acoustic particle velocity match the shell velocity $i\omega s_r$. This condition can be written in terms of a shell impedance

$$Z_{sh} = \left(\frac{p}{i\omega s_r}\right)_{r=a}$$

$$= -\frac{(\lambda + 2\mu)\ AH_0\ (A) - 4\mu H_1(A)}{i\omega a H_1(A)}, \quad (46)$$

where $A = k_{sh}a$. At $r = b$, we assume that we can estimate the effects of the surrounding fluid by using a radiation boundary condition. The shell boundary condition at $r = b$ is then

$$Z_r = \rho_g' c_g' \frac{i k_g' b}{1 + i k_g' b}$$

$$= -\frac{(\lambda + 2\mu) B H_0(B) - 4\mu H_1(B)}{i\omega a H_1(B)}, \quad (47)$$

where $B = k_{sh} b$ and ρ_g', c_g', and $k_g' = \omega/c_g'$ refer to the gas outside of the shell. In our work, this is the same as the gas inside the shell. However, it is useful to distinguish the two fluids so that our final expression can be applied to, e.g., liquid-filled resonators in an air environment.

Equation (47) can be used to evaluate the ratio of the constants in Eq. (45). When the results are used in Eq. (46), we obtain, after extensive algebra, an expression for the acoustic impedance of the shell at $r = a$. It is convenient to express this in the form of an acoustic admittance

$$\beta_{sh} = \rho_g c_g / Z_{sh} = [-i\rho\omega ca/(\rho_{sh} c_{sh}^2)]\, S_0(k_{sh} a), \quad (48)$$

where ρ_g and c_g refer to the gas inside the resonator. The function S_0 has the form

$$S_0 = -q[(G_1 + qRG_2)/(G_3 + qRG_4)], \quad (49)$$

where

$$q = (\lambda + 2\mu)/4\mu = \tfrac{1}{2}(1 - \sigma)/(1 - 2\sigma), \quad (50)$$

$$R = (\rho_g' c_g'^2 / \rho_{sh} c_{sh}^2)\, [(k_g' b)^2/(1 + i k_g' b)], \quad (51)$$

and

$$G_1 = (1 + AB - qB^2)\tan(B - A) - (B - A) - qAB^2,$$

$$G_2 = (1 + AB)\tan(B - A) - (B - A)$$

$$G_3 = [(qA^2 - 1)(qB^2 - 1) + AB]\tan(B - A)$$
$$\quad - (1 + qAB)(B - A),$$

$$G_4 = (1 + AB - qA^2)\tan(B - A) - (B - A) + qA^2 B.$$

$$\quad (52)$$

In Eq. (50), the second form expresses the ratios of the elastic constants in terms of Poisson's ratio σ.

At zero frequency, the radiation terms vanish and the admittance function S_0 is the limiting value of $-qG_1/G_3$:

$$S_0(0) = -q\frac{-3qab^2 + 3abh\,(a - qb) + h^3}{3qh\,(a^2 + ab + b^2) + 3abh + h^3}, \quad (53)$$

where $h = b - a$ is the shell thickness. The shell resonances occur at frequencies for which the denominator in Eq. (49) vanishes. If the radiation terms are neglected, the frequencies are given by the zeros of $G_3(k_{sh} a)$. The lowest root corresponds to the breathing mode of the shell. The higher frequency modes occur when $\tan(k_{sh} h)$ is close to zero. These modes correspond roughly to the longitudinal thickness modes of a flat plate. They clearly occur at much higher frequencies than the gas resonances as long as c_{sh}/h is much larger than c_g/a. This suggests that a good approximation to Eq. (49) can be obtained by simply dividing the zero frequency limit by a resonance term $[1 - (f/f_{br})^2]$, where f_{br} is the breathing resonance frequency. For the shell used in the present work, this "isolated mode" approximation does not differ from the exact result by more than about 2% except very close to the breathing resonance.

For the nonradial case, the shell admittance is given by an expression similar to Eq. (48), with S_0 replaced by a more general function S_n.[19] For $n > 0$, the admittance function S_n

TABLE I. Resonance frequency shifts and losses due to shell motion (argon at 296 K, 1 MPa).

s	f_{0s}/f_{br}	No radiation $10^6 \Delta f_{sh}/f_{0s}$	With radiation $10^6 \Delta f_{sh}/f_{0s}$	$10^6 g_{sh}/f_{0s}$
2	0.03	−51.96	−51.96	0.01
3	0.09	−55.46	−55.46	0.02
4	0.19	−61.72	−61.72	0.04
5	0.31	−72.71	−72.71	0.08
6	0.47	−93.67	−93.67	0.16
7	0.65	−143.71	−143.72	0.44
8	0.87	−386.57	−386.65	3.75
9	1.12	408.83	408.63	4.82
10	1.40	122.13	122.12	0.49

must be calculated numerically. For the present, we simply note the formal similarity of the radial and nonradial cases, and proceed to calculate the shifts in the resonance frequencies due to shell motion.

Equation (37), together with an expression for the shell admittance, can be used to determine the quantities $k_0 a$. These quantities represent the acoustic eigenvalues in the absence of dissipative and boundary-layer effects, but with the shell motion completely accounted for. For ω near cz_{ns}/a, the quantity $\rho\omega ca$ in Eq. (48) is approximately $\rho_g c_g^2 z_{ns}$, or approximately $\gamma P z_{ns}$ in the ideal-gas limit. For aluminum, the quantity $\rho_{sh} c_{sh}^2$ is about 1.1×10^6 MPa. The dimensionless function $S_n(k_{sh} a)$ is of order unity except for frequencies near shell resonances. Thus, for gases at moderate pressures, β_{sh} will have a small magnitude, and an approximate solution to Eq. (37) can be found by carrying out series approximations similar to Eqs. (40), with $k_0 a$ replaced by z_{ns}. This leads to

$$\frac{\Delta f_{sh} + i g_{sh}}{f} = \frac{-i\beta_{sh}/z_{ns}}{1 - n(n+1)/z_{ns}^2}$$

$$= \frac{\rho_g c_g^2}{\rho_{sh} c_{sh}^2} \frac{S_n(k_{sh} a)}{1 - n(n+1)/z_{ns}^2}. \quad (54)$$

The shell effects are largest at the highest pressures. Equations (49)–(52) and (54) have been used to calculate the shifts in the resonance frequencies of the radial modes of argon at 296 K and 1.0 MPa in the aluminum shell used in our work. The results are summarized in Table I. The imaginary terms represent radiation losses from the outside of the shell. Except for the $(s,n) = (0,8)$ and $(0,9)$ modes, which

TABLE II. Effects of shell dissipation on acoustic losses (argon at 296 K, 1 MPa).

s	f_{0s}/f_{br}	$10^6 g_{sh}/f_{0s}$ for $Q_{sh} =$			
		10	100	1000	10 000
2	0.03	0.96	0.10	0.01	0.00
3	0.09	1.88	0.19	0.02	0.00
4	0.19	3.29	0.33	0.03	0.00
5	0.31	5.90	0.59	0.06	0.01
6	0.47	11.94	1.21	0.12	0.01
7	0.65	32.28	3.40	0.34	0.03
8	0.87	187.20	28.53	2.87	0.29
9	1.12	207.21	36.44	3.67	0.37
10	1.40	34.09	3.70	0.37	0.04

are close to the breathing resonance of the shell, the radiation-loss term is negligible. The real part of the frequency shift is shown for the cases of a radiation load and for the case of a vacuum surrounding the shell. The numerical results in Table I are carried out to sufficiently high order to show that there is only a negligibly small difference. When the radiation effects are small, the ratio of the imaginary and real parts of S_0 is proportional to the external gas density. Equation (54) shows that the quantity $\Delta f_{sh} + i g_{sh}$ is proportional to the product of the density and S_0; thus Δf_{sh} is proportional to the density and g_{sh} is proportional to the square of the density. At a pressure of 0.1 MPa, the radiation loss terms become negligible even for the modes nearest the breathing mode of the shell. Because all the experimental work reported in this paper was carried out at pressures below 1 MPa, the radiation losses have been neglected in the remainder of our formal analysis.

It is also worth considering the effect of internal losses in the shell. The losses are associated with strain rates, and can be described in terms of complex elastic constants. In the isolated mode approximation, this leads to an expression of the form

$$S_0(f) = \frac{S_0(0)}{1 - (f/f_{br})^2 + i (f/f_{br})/Q_{sh}}, \quad (55)$$

where Q_{sh} is a shell quality factor. Table II summarizes the loss terms g_{sh}/f_{0s} for the radial modes for a pressure of 1 MPa and for various values of Q_{sh}. It is clear that the contributions will be significant only for very small values of Q_{sh} and for frequencies near the breathing resonance.

Numerical calculations of the admittance function $S_n(k_{sh}a)$ for the nonradial modes have been described elsewhere.[19] Results for the $n = 1$ modes of the aluminum shell used in our work are presented in a later section.

A qualitative discussion of the functional form of $S_n(k_{sh}a)$ is useful in the present context. For $n > 2$, the specific admittance of the shell is qualitatively similar to the $n = 0$ case, except for the additional bending mode resonances at lower frequencies (i.e., lower than f_{br}). At low frequencies, the admittance is the inverse of a stiffness reactance associated with the elastic deformation of the shell. For each n, as the frequency is increased, the shell inertia becomes more important, until the admittance diverges at the bending-mode resonance. For each n, there is an additional resonance at frequencies above f_{br}. These modes, like the breathing mode, are associated with a net stretching of the shell. At still higher frequencies, there are resonances which correspond to the longitudinal thickness modes of a flat plate.

For $n = 1$, the "bending" mode is at zero frequency. The displacement proportional to $Y_{1m}(\theta,\phi)$ is equivalent to uniform translation of the shell. For the $n = 1$ case only, the acoustic pressure exerts a net force on the shell which excites this translational motion. The corresponding inertial reactance can be easily calculated if deformation of the shell is neglected. The resulting specific admittance is given by

$$i(\omega a/c)\beta_{sh} = M_{gas}/M_{sh}, \quad (56)$$

where M_{gas} is the total mass of gas in the shell, and M_{sh} is the total shell mass. This equation is in close agreement with the

numerical calculations for frequencies well below the first nonzero, $n = 1$ shell resonance. The frequency shift corresponding to Eq. (56) is

$$(\Delta f_{sh}/f)_{1s} = (M_{gas}/M_{sh})/(z_{1s}^2 - 2), \quad (57)$$

which can be interpreted as a reduced mass correction for a coupled oscillator times a correction factor. The correction factor accounts for the difference between the actual fluid motion and uniform translational oscillations.

D. Holes in the shell

Vent holes through the resonator shell can be modeled as uniform cylindrical ducts with an appropriate terminal impedance. The same is true for holes which acoustically couple the inside of the shell to transducers which are either external or partially imbedded in the shell. The propagation parameter for waves in the duct is, according to the Kirchhoff–Helmholtz theory,[13,20]

$$k_{KH} = (\omega/c)\left\{1 + (1 - i)\left[(\gamma - 1)\delta_t + \delta_v\right]/(2r_h)\right\}, \quad (58)$$

where r_h is the duct radius. Let β_0 be the terminal specific admittance of a duct of length L. Then the input specific admittance of the hole, β_h, is given by

$$i\beta_h = (i\beta_0 - \tan k_{KH}L)/(1 + i\beta_0 \tan k_{KH}L). \quad (59)$$

For the vent hole, $i\beta_0$ can be estimated by assuming a radiation boundary condition appropriate for an opening with an infinite flange:

$$i\beta_{rad} = \left[\frac{8}{3\pi}\left(\frac{\omega r_h}{c}\right) - \frac{i}{2}\left(\frac{\omega r_h}{c}\right)^2\right]^{-1}. \quad (60)$$

Under typical conditions where $|i\beta_{rad}| > |\tan k_{KH}L|$, Eq. (59) simplifies to

$$i\beta_h = \cot k_{KH}L. \quad (61)$$

When typical experimental parameters are used in the evaluation of Eq. (59), the magnitudes of both the real and imaginary parts of $i\beta_h$ are found to be of order unity, except for frequencies near the resonance frequencies of the ducts. For a hole terminated by a transducer in a cavity with an effective volume V_c, the terminal specific admittance is given by

$$i\beta_c = -\omega V_c/(\pi r_h^2 c). \quad (62)$$

The transducer coupling hole has a Helmholtz resonance at low frequencies which can significantly perturb the eigenfrequencies of the lowest modes. The higher-frequency resonances occur very close to the frequencies for which an integral number of half-wavelengths equal the duct length. Thus, at higher experimental frequencies, $|i\beta_h|$ can be kept on the order of unity by using a sufficiently short duct. The vent hole is formed with a short duct of small radius coupled to a much larger duct drilled partway through the shell.

The effects of nonuniform boundary admittances on the eigenfrequencies can be calculated using boundary perturbation theory.[21] Let the unperturbed state correspond to the boundary condition (7) with $\beta(\omega)$ representing the terms in (34), and let $\beta(\omega, r_s) = \beta(\omega) + \Delta\beta(\omega, r_s)$. The additional shift in the eigenfrequency is given by

$$\frac{\Delta F_{ns}}{f} = \frac{i\omega a^2}{2cz_{ns}^2} \frac{\int_S \Psi_{ns}^2 \Delta\beta(\omega, \mathbf{r}_s) \, dS}{\int_V \Psi_{ns}^2 \, dV}, \tag{63}$$

where the Ψ_{ns} are eigenfunctions satisfying the boundary condition (7), the integral in the numerator is over the surface of the resonator, and the integral in the denominator is over the volume of the resonator. The shifts in the eigenfrequencies due to a hole in the shell can be easily calculated for the radial modes, since the eigenfunction is a constant on the shell wall. The result is

$$\frac{\Delta f_h + ig_h}{f} = \frac{i\beta_h}{z_{ns}} \frac{\Delta S}{4\pi a^2}, \tag{64}$$

where $\Delta S / (4\pi a^2)$ is the ratio of the area of the hole to the surface area of the shell. Typically this ratio is on the order of 10^{-5}. The total hole perturbation has a similar magnitude for frequencies well away from the hole resonances.

E. Seam between the hemispheres

The seam where the two hemispheres are joined in the construction of the spherical resonator should also be considered. Our description of the shell motion assumed a uniform isotropic shell. We have made no theoretical estimates of the effects of the joint between the hemispheres, and must rely on experimental evidence (presented later in this paper) to justify the simplifications made in our theory of the shell.

A small gap at the junction of the hemispheres could also affect the resonance frequencies. If the surfaces at the joint are smooth and fit well, it is reasonable to assume that the average width of the gap is less than δ_v. In this limit, the specific admittance can be estimated from the Poisueille flow resistance for a channel of uniform width. Assume the channel cross section is D by $2\pi a$, and the length is L. The corresponding specific admittance is real and equal to $\rho c D^2/(12\eta L)$. Thus there is no frequency perturbation; the contribution to the resonance width of radial modes is given by

$$g/f = \rho c D^3/(24\eta L a z_{0s}). \tag{65}$$

For argon at 300 K, 0.1 MPa, $D \approx 5 \, \mu m$, with the dimensions of the sphere used in this work, this is equal to $1.4 \times 10^{-8}/z_{0s}$, which is negligible.

F. Imperfect spherical geometry

The holes considered in the previous section are a type of geometric imperfection which has small dimensions compared with a typical acoustic wavelength. We now consider larger-scale geometric imperfections. Let the inner surface of the sphere be described by

$$\frac{r}{a} = 1 - \epsilon \sum_{lm} c_{lm} Y_{lm}(\theta, \phi), \tag{66}$$

where ϵ is a small parameter and the series represents a shape factor with a magnitude of order unity. Boundary shape perturbation theory[22] can be used to calculate the shifts in the eigenfrequencies in terms of the coefficients c_{lm}. In interpreting the results, it is useful to adjust the value of c_{00} so that the effects of change of volume are not included. That is, we wish to consider relative changes in the eigenfrequencies as the sphere is distorted, subject to the constraint that the volume does not change. Then, for radial modes, the effect of change

of shape alone causes fractional shifts in the eigenfrequencies which are of order ϵ^2. Greenspan[18] demonstrated this for spheroidal deformations by expanding the exact solution, and Mehl[23,24] showed it for arbitrary shapes using perturbation theory. The numerical prefactor $\Delta f/(f\epsilon^2)$ depends on the shape but is typically of order unity. Some values are tabulated in Ref. 23.

A complete discussion of the case of nonradial modes is presented elsewhere.[24] The results will be summarized here, particularly for the $n = 1$ case. For nonradial modes, the lowest-order shift in the eigenfrequencies is linear in ϵ. Consider the $n = 1$ case. Owing to symmetry, the matrix elements of boundary shape perturbation theory vanish except for the terms corresponding to the coefficients c_{lm} with l equal to 0 and 2. We disregard the $l = 0$ term which describes a change in volume, since this term leads to the same shift for all modes.

It is worth considering the types of shape imperfections which are likely to arise in machining and assembling a resonator from two hemispheres. The individual parts are likely to have a high degree of rotational symmetry about their respective axes, and to be cut off in a plane which is accurately perpendicular to the axis of symmetry. However, the distance of the cutoff plane from the "pole" of the hemisphere must be measured by the machinist. It is probable that actual parts may be cut off a bit long or a bit short. Such effects can be described by a term of the form $-\epsilon P_2(\cos\theta)$ in Eq. (66). The mean radii of the two parts are also likely to differ by a small amount. This type of perturbation can be described by odd-order Legendre polynomials in Eq. (66). Owing to symmetry, such terms do not shift the eigenfrequencies to first order. A third type of fabrication error is likely to arise in assembly of the resonator. The axes of symmetry of the two parts are likely to be quite parallel, but not necessarily coincident. Let the separation of the two axes be $2\epsilon_1 a$. This leads to terms in Eq. (66) with $m = 1$. The only terms which contribute to a perturbation of the $n = 1$ eigenfrequencies are those in

$$r/a = 1 - \epsilon_0 P_2(\cos\theta) - \tfrac{5}{8}\epsilon_1 P_2^1(\cos\theta)\cos\phi. \tag{67}$$

The corresponding frequency shifts are

$$\frac{\Delta f_{geom}}{f} = \frac{\epsilon_0}{5} \frac{z_{1s}^2 + 1}{z_{1s}^2 - 2} \lambda, \tag{68}$$

where λ is an eigenvalue of a 3 by 3 matrix. The eigenvalues are

$$\lambda_0 = 0,$$
$$\lambda_{\pm 1} = \tfrac{1}{2} \pm \tfrac{3}{2} \left[1 + \tfrac{25}{16}(\epsilon_1/\epsilon_0)^2 \right]. \tag{69}$$

Note that when $\epsilon_1 = 0$, the degeneracy is only partly lifted. The mode with angular factor $\cos\theta$ corresponds roughly to translational motion along the z axis. The eigenvalue for this mode is $\lambda_{+1} = 2$. The frequency is determined mainly by the polar diameter of the resonator, which, according to Eq. (67), is decreased by a fractional amount ϵ_0. The modes with angular factors $\sin\theta\cos\phi$ and $\sin\theta\sin\phi$ correspond roughly to translational motion along the x and y axes. Their eigenfrequencies are determined by the equatorial diameter, which is increased by a fractional amount $-\epsilon_0 P_2(0)$

$= \epsilon_0/2$. When ϵ_1 is nonzero, the degeneracy of these modes is lifted. One of the frequencies of the degenerate modes is unchanged since the effective length of the resonator in the y direction is not changed by a small displacement $2\epsilon_1 a$ in the x direction. The eigenfunctions of the $+1$ mode and the -1 mode get mixed somewhat, and the frequencies move further apart. The -1 mode will correspond to translational motion along the long axis of the resonator, which will be at some angle to the z axis.

The splitting of nonradial modes by boundary shape perturbations is of interest because it permits a measure of the geometric quality of the resonator directly from acoustic measurements. The nsm modes of a perfect resonator are $(2n + 1)$-fold degenerate; thus the analysis of the data becomes increasingly complicated as n increases. On the other hand, the higher n modes yield information about the higher-order coefficients in Eq. (66).

G. Steady-state response

The steady-state response of the resonator can be calculated using a Green's function. To lowest order, the acoustic pressure $p(\mathbf{r})$ is a solution of the Helmholtz equation (3) and satisfies the boundary condition given by Eq. (4) on the entire boundary except for a small active region S'. On this source region, let the sum of the normal component of the gas velocity and $\beta p/(\rho c)$ equal the source velocity u_s, so that

$$\frac{\partial p}{\partial n} = -i\left(\frac{\omega}{c}\right)\beta p - i\omega\rho u_s. \tag{70}$$

Let the Green's function be the solution of

$$(\nabla^2 + \omega^2/c^2)\, G\,(\mathbf{r},\mathbf{r}') = \delta(\mathbf{r} - \mathbf{r}'), \tag{71}$$

which satisfies the boundary condition

$$\frac{\partial G}{\partial n} = i(\omega/c)\,\beta\,(\omega,\mathbf{r})\, G\,(\mathbf{r},\mathbf{r}')$$

for $\mathbf{r}$ on the surface S. Use of Green's theorem leads to

$$p\,(\mathbf{r}') = \int_s \left(p\,\frac{\partial G}{\partial n} - G\,\frac{\partial p}{\partial n}\right) dS$$

$$= i\omega\rho \int_{s'} G\,(\mathbf{r},\mathbf{r}')\, u_s\,(\mathbf{r})\, dS. \tag{72}$$

The eigenfunction expansion of the Green's function is

$$G\,(\mathbf{r},\mathbf{r}') = \sum_N \frac{\Psi_N(\mathbf{r})\, \Psi_N(\mathbf{r}')}{4\pi^2 V\Lambda_N\,(f^2 - F_N^2)/c^2}, \tag{73}$$

where Λ_N is the average value of Ψ_N^2 over the volume V. Equations (72) and (73) lead to

$$p\,(\mathbf{r}') = \sum_N \frac{if\rho c^2\Psi_N(\mathbf{r}')}{2\pi V\Lambda_N\,(f^2 - F_N^2)} \int_{s'} \Psi_N(\mathbf{r})\, u_s\,(\mathbf{r})\, dS. \tag{74}$$

The detector is typically a pressure transducer whose complex output voltage $u + iv$ is proportional to $p\,(\mathbf{r}')$, and is hence proportional to the summation in Eq. (74). In normal experimental practice, only one or a small number of modes whose eigenfrequencies lie within a small range are excited. The contribution of the excited modes can be described in detail by including one or a small number of terms in the summation in Eq. (74). The remaining terms of the summation can be approximated using a Taylor series in frequency. The detector output can then be written

$$u + iv = \sum_N \frac{ifA_N}{(f^2 - F_N^2)} + B + C\,(f - f_0), \tag{75}$$

where A_N, B, and C are complex constants, and the sum is now over only one mode or over a small number of modes of interest. The remaining modes contribute to the background terms proportional to B and C. As long as the shell is fairly rigid, the eigenfrequencies $F_N = f_N + ig_N$ in Eq. (75) are given to sufficient accuracy by

$$f_{nsm} = cz_{ns}/2\pi a + \Delta f_t + \Delta f_v + \Delta f_{sh} + \Delta f_h + \Delta f_{geom}, \tag{76}$$

$$g_{nsm} = g_t + g_v + g_h + g_{bulk}, \tag{77}$$

where $\Delta f_t + ig_t$ and $\Delta f_v + ig_v$ are equal to the terms in Eq. (41) which are proportional to β_t and β_v, respectively, Δf_{sh} is given by Eq. (54), Δf_h and Δg_h represent the sum of all hole contributions, each of the form (64), and g_{bulk} is given by Eq. (39).

Equation (75) represents the steady-state response of the resonator to a source with a frequency f. When the source is turned off, the signal decays away exponentially. As long as the energy of the shell motion is a small fraction of the energy of the gas motion, the decay will be proportional to $\exp(-2\pi g_{nsm}t)$, where g_{nsm} is given by Eq. (77). (If the shell energy were large enough, we would have to include a distributed source over the boundary at $r = a$ in our description of the gas.) For the $n = 0$ modes, the ratio of the shell energy to the gas energy can easily be shown to be $(h/a)\,(\rho_{sh}/\rho_g)|\beta_{sh}|^2$. Except for the case of a gas resonance nearly coincident with the breathing mode of the shell, for our resonator at pressures less than 1 MPa, this ratio is less than 10^{-8}.
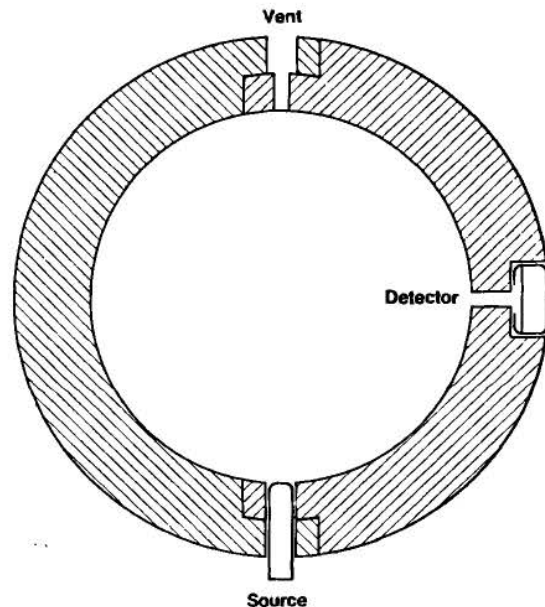

FIG. 1. Cross section of resonator shell (not to scale) showing orientation of vent, transducers, and seam. The inner diameter of the shell is 12.7 cm and the shell thickness is 1.24 cm. The two parts of the shell are held together by bolts, which are not shown.

II. EXPERIMENTS

A. A prototype resonator

The data reported below were all taken with the resonator sketched in Fig. 1. This resonator was assembled from two hemispheres. The hemispheres were milled from cylindrical stock of aluminum 6061. (In an earlier publication,[2] this resonator was incorrectly described as being made from aluminum 2024.) The nominal inner diameter is 12.7 cm and the nominal wall thickness is 1.24 cm. Conventional mechanical metrology just following the machining of the resonator parts showed that the resonator had an average inside diameter of 12.6975 ± 0.0025 cm.[25] The deviations from sphericity of each hemisphere were about 0.0005 cm, a tolerance which is much finer than required for accurate measurements. The hemispheres differed in average diameter by 0.0042 cm. In several years of use before the experimental work reported here was carried out, the resonator was disassembled and re-assembled many times, and additional minor machining was carried out. No recent direct measurements of the sphere shape have been made. The step where the hemispheres meet was intended to insure that they remain coaxial within 0.0025 cm when they are bolted together. The mating surfaces on the step were lapped and the interior surfaces were polished with #600 paper prior to assembly.

The homemade source transducer is sketched in Fig. 2. It fitted snugly in a 0.3-cm-diam hole through the resonator shell. The active surface was approximately flush with the interior surface of the shell. This transducer was driven with 150-V rms ac and no dc bias. Thus it operated as a "square law" device generating an acoustic signal at double the frequency of the electrical excitation. This strategy insured that the electrical crosstalk between the transmitter and receiver was negligible. The small mass of the vibrating aluminized mylar minimized mechanical crosstalk between the transmitter and the receiver.
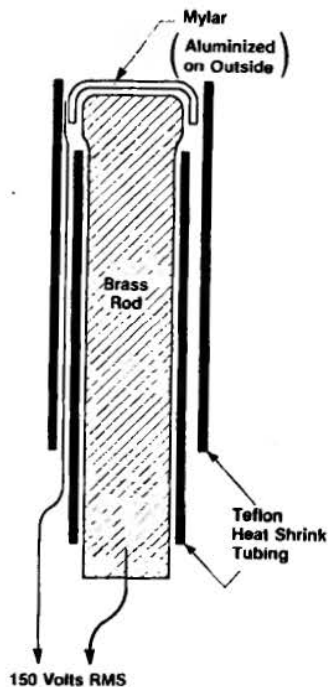

FIG. 2. Schematic diagram of source transducer. The transducer is 0.35 cm in diameter and 1.7 cm long.

The detector was a commercially manufactured electret microphone with a built-in FET amplifier. A porous shield was removed from the front of this small (0.62-cm-diam by 0.50 cm long), inexpensive (less than $5) device. The detector was then pressed into the machined hole in the shell (see Fig. 1). A duct (0.079-cm-diam and 0.64 cm long) led from the detector to the interior of the shell. This duct acts as the acoustic inductance of an unintended Helmholtz resonator. The acoustic capacitance of this resonator was the small volume within the aluminum case of the microphone in front of the electret disk. The frequency of this resonator is near 3.1 kHz (in air) and has a Q of about 3. Unfortunately, this resonance is close to the lowest radially symmetric mode of oscillation of the gas within the spherical shell, and perturbs the gas resonance significantly.

The FET in the detector was biased with a 1.5-V battery. The resulting 1-mW dissipation does not produce a significant temperature gradient in the shell.

The source transducer approximates a point source. The detector transducer is deliberately placed at 90° with respect to the source; thus its efficiency for detecting the symmetry-forbidden $(n,s) = (3,1)$ resonance is greatly reduced in comparison with its efficiency for detecting the nearby, radially symmetric (0,2) resonance.

The vent hole through the resonator's shell was divided into two sections, as illustrated in Fig. 1. The inner section was 0.078 cm in diameter and 0.64 cm long. The outer section was 0.32 cm in diameter and 0.64 cm long. If a single, straight hole had been used, its resonance (considered as an open organ pipe) would fall quite close to the (0,5) resonance of the gas-filled shell. The perturbation produced by such a vent on the (0,5) resonance would be difficult to calculate to the desired accuracy. We have previously observed that such organ-pipe resonances appear to drive shell motion, leading to spurious coupling of the source and the detector.[2]

No effort was made to make the resonator gastight. Instead, it was enclosed in a pressure vessel which also functioned as the innermost stage of a multistage thermostat. Details of the thermostat have been published elsewhere.[2] All the data were taken at temperatures within 5 mK of 296.310 K. Small corrections were made to reduce all data to this temperature.

In addition to the 1-liter aluminum resonator just described, we have extensive experience with a 1/8-liter brass resonator. No new phenomena were encountered with the smaller resonator.

B. Gas properties

We have used a variety of gases in these resonators. They include argon, neon, helium, ethylene, propane, and the refrigerants bromotrifluoromethane (R13B1) and 1,1 difluoroethane (R152a). For this paper, our argon data are the most relevant. The argon which we used was stated to be 99.9999% pure by the manufacturer. The pressure vessel was pumped and flushed extensively; however, it was not baked out. Speed of sound measurements at pressures down to 10 kPa (not discussed here) suggest that a volatile impurity (such as water vapor) degassed from the interior of the

pressure vessel until it reached a partial pressure on the order of 1 Pa. Such an impurity will not have a major effect on the data discussed here.

The properties of argon are summarized in Table III. The viscosity was obtained from the accurate measurements of Kestin et al.[26] The thermal conductivity K was obtained from the viscosity η by using the Eucken equation

$$K/(C_p\eta) = (9\gamma - 5)/(4\gamma), \qquad (78)$$

where γ is the ratio of the specific heats. The thermal conductivity determined in this way is consistent with less accurate direct measurements.[27] The density was obtained from our pressure measurements through the virial equation. Our expression for the virial coefficients $B(T)$ is based on the model fit to argon data by Sengers, Klein, and Gallagher.[28,29] The pressure dependence of the speed of sound was written as a truncated Taylor series:

$$c(T,P)^2 = \gamma RT/M + A_1(T)P + A_2(T)P^2. \qquad (79)$$

The coefficient A_1 was obtained from the thermodynamic relation

$$A_1(T) = \frac{\gamma}{M}\left(2B(T) + 2(\gamma - 1)T\frac{dB(T)}{dT}\right.$$
$$\left. + \frac{(\gamma - 1)^2}{\gamma}T^2\frac{d^2B(T)}{dT^2}\right). \qquad (80)$$

Analytic expressions for the derivatives in Eq. (80) were obtained from the work of Gallagher and Klein[29]; the polynomial representation in Table III is a fit to their results. For A_2, we used the value 5.45×10^{-11} m^2/s^2/MPa^2, which best fits our data and which is consistent with the direct measurements of the speed of sound made by El-Hakeem[30] at pressures up to 7 MPa where the influence of A_2 is much greater.

Our experiences with propane have led us to discuss precondensation phenomena elsewhere.[12] We remark that the refrigerant R152a is particularly convenient for studying resonators at low frequencies. It has a small value (0.14) for $\gamma - 1$ and rapid intramolecular relaxation leading to very high Q's. (At 0.1 MPs, the Q's of the 15 lowest radially symmetric modes all exceed 10 000.)

C. Spectrum of resonances

When the frequency of the source is swept slowly, the amplitude of the detected signal reveals the spectrum of resonances discussed by Rayleigh[31] (see Fig. 3). When the shell is considered to be a perfect, rigid, insulating sphere and the viscosity and the thermal conductivity of the gas are neglected, the resonance frequencies are equal to
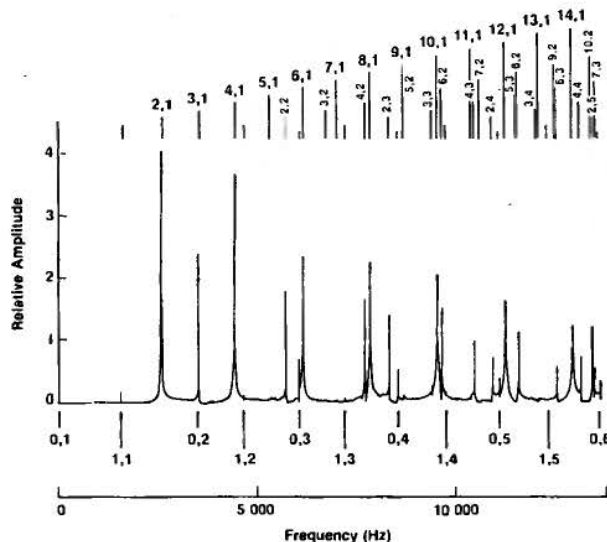
TABLE III. Properties of argon.

$M = 0.039\,947\,6$ kg/mole
$A_1 = (2.724 - 1.834/T^* - 0.685/T^{*2}) \times 10^{-3}$ m^2/s^2/MPa
$A_2 = 5.45 \times 10^{-11}$ m^2/s^2/MPa^2
$\rho = \dfrac{MP/(RT)}{1 + BP/(RT)}$
$B = (0.3454 - 4.3607/T^* - 0.1270/T^{*2}) \times 10^{-4}$ m^3/mole
$\eta = [2.1001 + 1.7482\,(T^* - 1) + 0.0020P^*/T^*] \times 10^{-5}$ Pa s
$T^* = T/(273.15\text{ K})$
$P^* = P/(0.1\text{ MPa})$

FIG. 3. Spectrum showing frequencies and relative amplitudes of the 40 lowest frequency modes in argon near 0.1 MPa and 296 K. The 0,s and 1,s modes which are studied in this paper are labeled just above the abscissa.

$cz_{ns}/(2\pi a)$. We recall that n denotes the order of the spherical Bessel function in Eq. (6) and s labels the roots z_{ns} in ascending order. Figure 3 displays the spectrum observed with the shell filled with argon near 0.1 MPa. The $(0,s)$ and $(1,s)$ modes which we studied in greatest detail are labeled just above the abscissa. Their eigenvalues and frequencies are listed in Table IV.

D. The dominant perturbations

Here, we review the dominant perturbations to the spectrum of resonances just described. These perturbations are needed to understand our data.

The resonator shell has both a high thermal diffusivity and a high heat capacity per unit volume compared with those of the gas. The adiabatic sound wave in the gas becomes an isothermal wave near the shell. This perturbs the resonance frequencies by

$$\frac{\Delta f_t + ig_t}{f} = \frac{-1 + i}{2a}\frac{(\gamma - 1)\sqrt{D_t/(\pi f)}}{1 - n(n + 1)/z_{ns}^2}, \qquad (81)$$

where D_t is the thermal diffusivity of the gas, which is equal to the thermal conductivity divided by the constant pressure heat capacity per unit volume.

TABLE IV. Eigenvalues and resonance frequencies at 296 K, $P = 0$.

s	z_{0s}	z_{1s}	f_{0s} (Hz)	f_{1s} (Hz)
1	0.000 000	2.081 576	0	1 673
2	4.493 409	5.940 370	3 611	4 774
3	7.725 252	9.205 840	6 208	7 398
4	10.904 122	12.404 445	8 763	9 969
5	14.066 194	15.579 236	11 304	12 520
6	17.220 755	18.742 646	13 839	15 062
7	20.371 303	21.899 697	16 371	17 599
8	23.519 453	25.052 825	18 901	20 133
9	26.660 543	28.203 361	21 425	22 665
10	29.811 599	31.325 092	23 958	25 196

For our resonator, Eq. (81) is approximately

$$\frac{\Delta f_t + ig_t}{f} = \frac{2.26\times10^{-4}(-1+i)/\sqrt{P^*f^*}}{1-n(n+1)/z_{ns}^2}. \quad (82)$$

(Here we have chosen to measure frequency in units of $f_{0,2}$ and pressure in units of 0.1 MPa; thus $f^* = f/3611$ Hz and $P^* = P/0.1$ MPa.)

For the nonradial modes of indices (n,s) with $n>0$, the boundary condition that the tangential component of the acoustic velocity vanish at the shell leads to a perturbation which depends upon the viscous diffusivity, $D_v = \eta/\rho$:

$$\frac{\Delta f_v + ig_v}{f} = \frac{-1+i}{2a}\frac{n(n+1)\sqrt{D_v/(\pi f)}}{z_{ns}^2 - n(n+1)}, \quad (83)$$

which, for our prototype resonator, can also be expressed in terms of P^* and f^* as

$$\frac{\Delta f_v + ig_v}{f} = \frac{2.76\times10^{-4}(-1+i)n(n+1)/\sqrt{P^*f^*}}{z_{ns}^2 - n(n+1)}. \quad (84)$$

The contribution to the half-width resulting from bulk dissipation throughout the volume of the resonator is given by Eq. (39). For our conditions, this is equal to

$$g_{bulk}/f = 3.6\times10^{-6}f^*/P^*. \quad (85)$$

The effects of shell motion on the acoustic modes can be described most easily by considering the $n=0$ and $n=1$ cases separately. For $n=0$ and at low frequencies, the acoustic pressure tends to stretch the shell, and the shell response is governed by an elastic stiffness. At higher frequencies, the inertial reactance of the shell grows. The stiffness and inertial reactances are equal at the breathing resonance of the shell near 20.2 kHz. The scale of the corresponding perturbations can be estimated from the thin-shell limit of Eqs. (49)–(54):

$$\frac{\Delta f_{sh}}{f} = -\frac{(\rho c^2)_g}{(\rho c^2)_{sh}}\frac{a/h}{2-(c/c_{sh})^2 z_{0s}^2}, \quad (86)$$

where a is the shell's radius, h is the shell thickness, and the subscripts "sh" and "g" refer to the shell and the gas, respectively. For our prototype resonator, the somewhat more accurate expression based on the isolated mode approximation leads to

$$\frac{\Delta f_{sh}}{f} = \frac{-5.0\times10^{-6}P^*}{1-(f/20.2\text{ kHz})^2}, \quad (87)$$

which predicts a divergent perturbation at the 20.2-kHz breathing mode resonance of the empty shell.

Entirely different phenomena occur at low frequencies with the $n=1$ modes. Because the acoustic pressure is proportional to $Y_{1m}(\theta,\phi)$, the gas exerts a net transverse force on the shell which excites translational motion. There is little deformation of the shell at low frequencies. The main effect is inertial. In practice, the frequency correction for shell motion must be calculated numerically.[19] At low frequencies, however, the approximate result given as Eq. (57) can be interpreted as a "reduced mass" correction.

E. Data aquisition and analysis

In order to measure the frequencies f_N and half-widths g_N of the radially symmetric modes with sufficient resolution, the following procedure was adopted. First, f_N and g_N were estimated from rough measurements. Then, the drive transducer was stepped through 11 synthesized, discrete frequencies starting at $f_N - g_N$ and increasing in increments of $g_N/5$ until $f_N + g_N$ was reached. At each frequency, the in-phase voltage u and the quadrature voltage v produced by the detector were measured with a tracking lock-in amplifier, scanner, and digital voltmeter, all operating under control of a microcomputer. Then, the sign of the frequency increment was reversed and the voltages were measured again as the frequency was reduced in steps back to its original value. The 11 frequencies and 44 voltages were fitted by a function of the theoretically predicted form [Eq. (75)] using the efficient algorithm previously described.[32] For radially symmetric modes, the sum in Eq. (75) is replaced by a single term representing the radial mode under study. A small number of terms were used in the sum when studying nonradial modes. The fit determines values of the complex resonance frequencies $F_N = f_N + ig_N$, the complex amplitudes A_N (this allows for undetermined phase shifts in the source–detector path), and the complex "background" parameters B and C allow for the influence of the tails of all of the resonances other than the particular ones under study. In almost every case, all of the measured voltages fit Eq. (75) with a precision of better than 0.1% of the maximum voltage. It follows that f_N is determined by the fit with a preci-
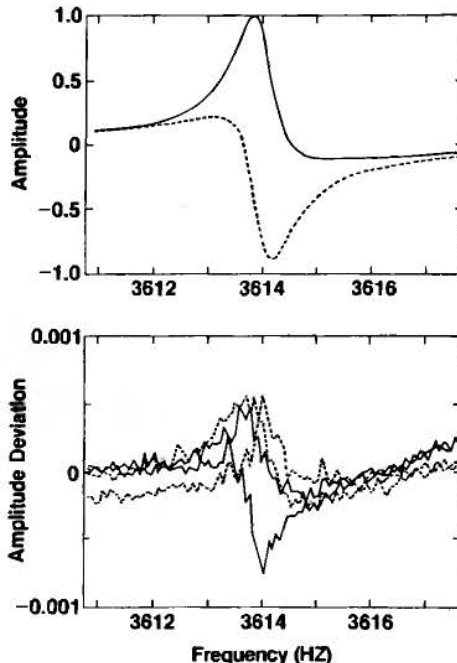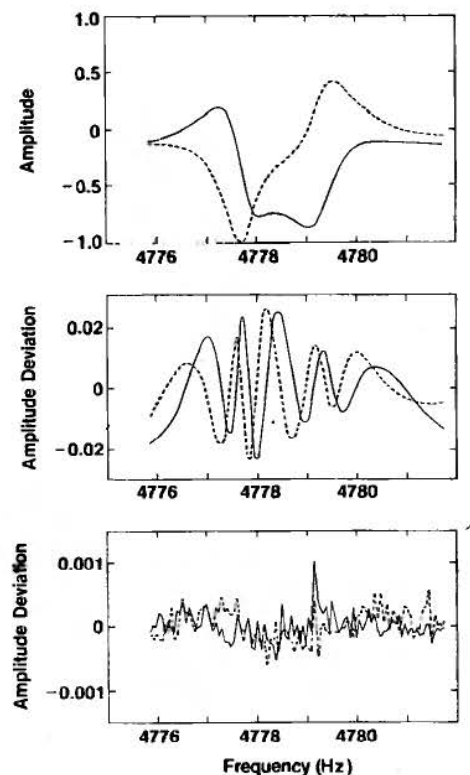

FIG. 4. Top: In-phase (solid curve) and quadrature (dashed curve) voltages from the detector as a function of frequency near the (0,2) resonance in argon at 0.4032 MPa and 296.309 K. Bottom: Measured voltages minus calculated voltages [Eq. (75)] with the fitted parameters $f_{02} = 3613.9970$ Hz, $g_{02} = 0.4275$ Hz, $A = 0.7535 - 0.5831i$, $B = 0.0048 + 0.0068i$, and $C = 0.0001 + 0.0001i$. Data were taken at intervals of 0.07 Hz, first from the lowest to the highest frequency and then back to the lowest frequency. Separate deviation plots for the upward and downward frequency sweeps show the effects of drifts in the lock-in amplifier.

sion of 0.1% of g_N or typically 10^{-7} of f_N. This precision is a factor of five greater than that required to measure the gas constant to 1 part in 10^6.

An important check of the entire data acquisition system and the numerical methods used to fit Eq. (75) to the data was made when the resonator was filled with propane at 287.5 K and 0.52 MPa. Under these conditions, the (0,2) mode occurs at 2568 Hz and has a half-width of 0.0526 Hz. We excited this mode, turned off the excitation, and measured the detected voltage as a function of time during the "ring down." The value of $g_{0,2}$ determined by fitting an exponential form to the decay curve differed from the value determined by cw methods by only 0.0004 Hz, or $1.6 \times 10^{-7} f_{0,2}$.

It is of some interest to demonstrate that the resonances do indeed have the theoretically predicted form [Eq. (75)] over a wider range of frequencies and with greater precision than that required to measure f_N. Figure 4 is such a demonstration. Voltages were measured near the (0,2) resonance at 100 frequencies spanning the range $\pm 8g_N$. All of the data fit the theoretical form within 0.08%; the rms deviation is 0.013%. To this extent, the resonator does behave like our theoretical model. Nevertheless, the deviations from the fit systematically exceed the noise. We believe these small deviations result from small phase drifts within the lock-in am-

FIG. 5. Top: In-phase (solid curve) and quadrature (dashed curve) voltages from the detector as a function of frequency near the (1,2) resonance in argon at 0.4032 MPa and 296.309 K. Middle: Measured voltages minus two-resonance trial function. Note that the deviations are systematic although the trial function has twelve parameters [eight parameters specify resonances at 4777.63 and 4779.38 Hz, and four specify the constant and linear background terms in Eq. (75)]. Bottom: Measured voltages minus fitted function. The fitted function has sixteen parameters [twelve parameters specify resonances at 4777.693, 4777.903, and 4779.351 Hz with half-widths of 0.550, 0.546, and 0.555 Hz. The remaining four parameters specify B and C in Eq. (75)].

plifier. (0.03° would be sufficient.) In future work this hypothesis could be tested using ac-bridge techniques as an alternative to a lock-in amplifier. Other possible contributions to the deviations could arise from very small temperature shifts (0.1 mK) or instabilities in the transducers during the 20 min needed to acquire the data.

It is necessary to pause at each frequency prior to a voltage measurement for a time which is a multiple of the slowest relaxation time of the measurement system. This may be either $1/g_N$, or the post-detection time constant of the lock-in amplifier, or the settling time of the frequency tracking circuitry of the lock-in amplifier. In practice, the time required to dwell at all 22 steps is several minutes. A small drift in the gas temperature during this interval will not affect the measurement of f_N very much; however, it would lead to serious errors in the measurement of g_N if we did not compensate for it by the practice of taking data stepping up and down in frequency.

In order to measure the frequencies and half-widths of the triply degenerate (1,s) modes, substantially more data are required than we routinely used to study the nondegenerate (0,s) modes. Figure 5 displays a typical set of measurements near the (1,2) modes. Again, data have been taken at 100 discrete frequencies. The data stepping up and down in frequency have been averaged for clarity. A casual inspection of the top of Fig. 5 suggests that the (1,2) mode is split into two components, one near 4477.6 Hz and one near 4479.3 Hz. The middle frame of Fig. 5 shows the deviations which result when a vector sum of two resonance terms and a complex (linear) background is fit to the data. This function is obviously unsatisfactory although it has 12 parameters (four for each resonance term and four for the background) which were adjusted to best fit the data in the sense of least squares. The lower frame of Fig. 5 shows that a satisfactory fit can be obtained when the 16 parameters required to represent the vector sum of three resonance terms and a complex
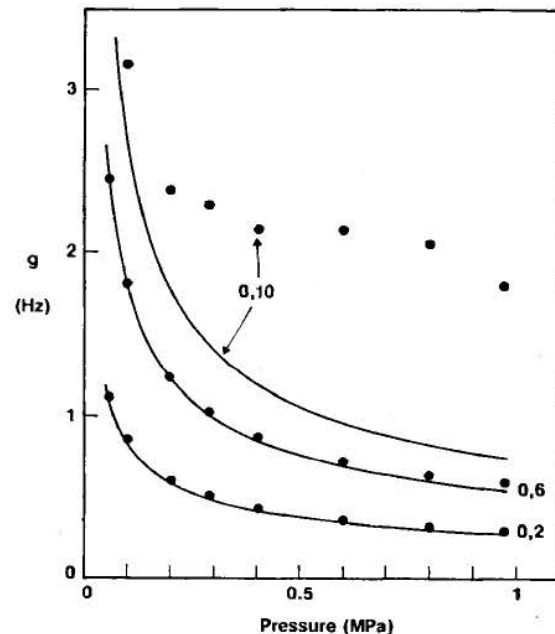

FIG. 6. Measured (dots) and calculated (curves) half-widths of three resonances as a function of pressure.

linear background are used to fit the data. The rms deviation of this fit (0.021%) is comparable to that obtained by fitting data for the (0,2) mode under similar conditions. Thus data of this quality and quantity can be used to resolve all three components of the nearly degenerate (1,2) modes. Our ability to do so depends upon having phase sensitive detection and upon the coincidence that all three components have roughly the same amplitude when they are studied with our transducer configuration. (The amplitudes are in the ratio 7.7:5.0:3.2.)

F. The resonance half-widths

Our data concerning resonance half-widths provide an important indicator of our understanding of gas-filled spherical resonators because these data can be compared to theory using thermal conductivity data and viscosity data derived from nonacoustic measurements. There are no unknown parameters which can be adjusted to improve the agreement between the data and the theory.

As an example, Fig. 6 compares the measured and the calculated half-widths for the (0,2), (0,6), and (0,10) modes at various pressures. The calculation for the half-widths includes the effect of the thermal boundary layer between the gas and the shell and the effect of bulk dissipation.

The measured half-widths always exceeded the half-widths calculated from the sum of Eqs. (81) and (39) as one would expect if there were other loss mechanisms. The excess half-widths are shown in Fig. 7. We have chosen to scale this half-width excess by the measured resonance frequencies to facilitate later comparison with frequency differences at a level of parts per million.

From Fig. 7, it is clear that the measured half-widths of the first five radially symmetric modes exceed the calculated
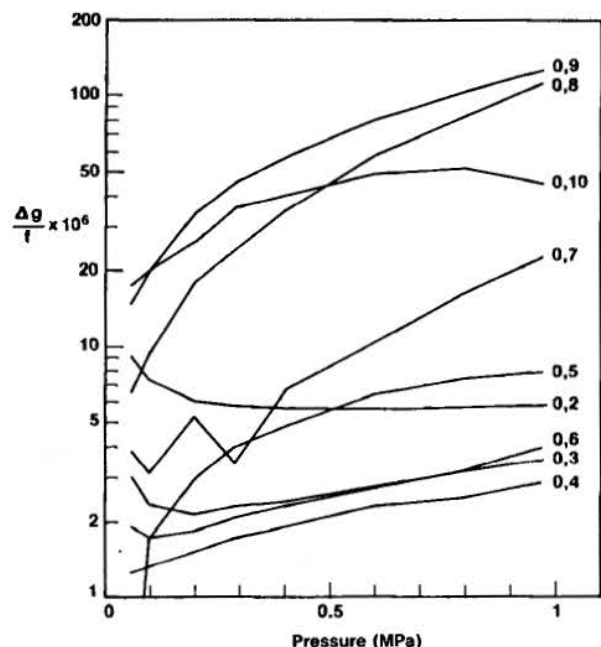
half-widths by less than 10 parts per million of the resonance frequency. In general, the excess grows as the pressure is increased and as the frequency is increased towards the shell's breathing resonance at 20.2 kHz between the (0,8) and (0,9) modes. Both of these trends are consistent with the idea that much of the excess half-width results from dissipation associated with the elastic response of the shell to the acoustic pressure. Friction in the joint between the hemispheres is a possible site for dissipation. The excess half-width for the (0,2) mode shows a different trend. We suspect this is a result of the proximity of the (0,2) mode to the Helmholtz resonance associated with the detector transducer and the duct connecting it to the interior of the shell.

In Fig. 8, the excess half-widths for the (1,s) modes are shown. The calculation for these modes includes the additional contribution to the half-width given by Eq. (83). The excess half-widths of most of the (1,s) modes are small and they increase very slightly with pressure. The excess half-widths for the (1,1) and (1,9) modes are both very large and very pressure dependent. These modes are expected to couple strongly to shell resonances which have the same symmetry and frequency as the gas motion. It is interesting to note that the frequency of the (1,8) mode is nearly coincident with the predicted frequency of the breathing mode of the shell; however, the coupling is not expected to be strong because they differ in symmetry. In agreement with this idea, there is only a small pressure-dependent excess half-width for the (1,8) mode. We were unable to measure the excess half-widths for the (1,5) modes above 0.4 MPa because the detected signal was too weak to reliably resolve the three components of this mode.
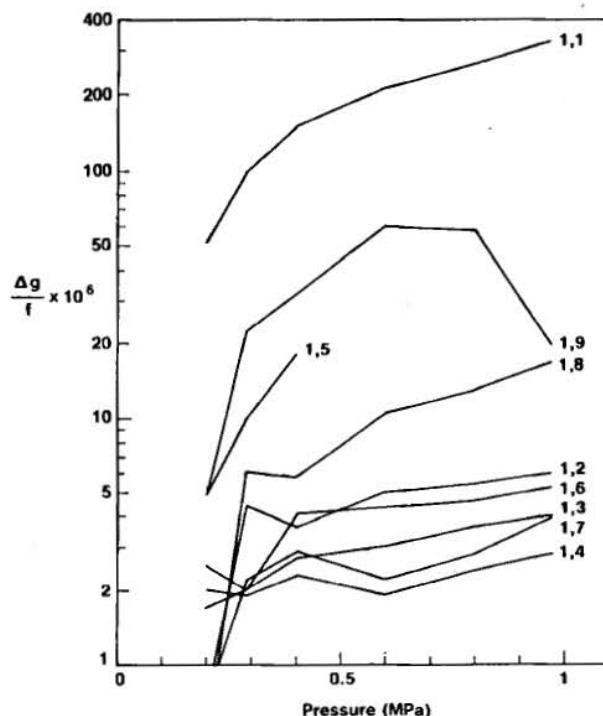

FIG. 7. Excess half-widths of (0,s) resonances (scaled by 10^6/frequency). Δg = measured g_N minus calculated g.

FIG. 8. Excess half-widths of 1,s resonances (scaled by 10^6/frequency). For each (1,s) resonance, Δg is obtained by subtracting the calculated half-widths from the average of the measured half-widths of the three components.

267   J. Acoust. Soc. Am., Vol. 79, No. 2, February 1986
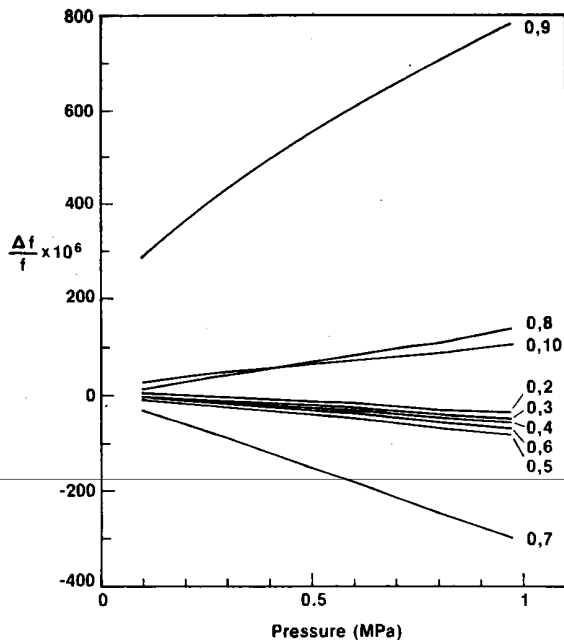
Moldover *et al.* : Spherical resonators   267

FIG. 9. Measured resonance frequencies minus calculated frequencies (scaled by 10^6/frequency) for $(0,s)$ modes. Here, the calculation includes the effect of the thermal boundary layer and holes in the resonator; however, the calculation omits the effect of shell motion. The linear dependence of $\Delta f / f$ on pressure is a result of shell motion. The slopes depend upon the proximity of the gas resonances to the shell breathing resonance near 20.2 kHz.

In summary, almost all the resonance half-width data can be accurately explained by a model which includes the viscothermal boundary layer and the dissipation within the bulk of the gas. When a gas resonance happens to fall near a shell resonance, a large, pressure-dependent excess half-width is observed.

G. The resonance frequencies and shell response

The Introduction emphasized that all of the resonance frequencies could be predicted if two parameters $c_0/(V_0)^{1/3}$ and A_2 were fit to one mode at two pressures and if our theoretical model were complete. In this section, we shall illustrate the extent to which this is true when the model includes the effects of the viscothermal boundary layer [Eqs.
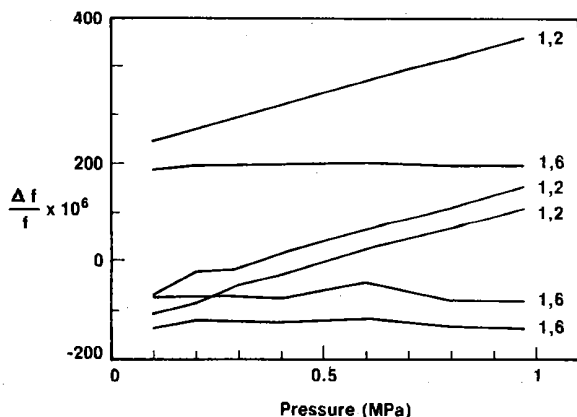
FIG. 10. Measured resonance frequencies minus calculated frequencies (scaled by 10^6/frequency) for the three components of the $(1,2)$ and $(1,6)$ resonances. Here, the calculation includes the effect of the viscous and thermal boundary layers; however, neither the effects of shell motion nor the effects of the holes are included.
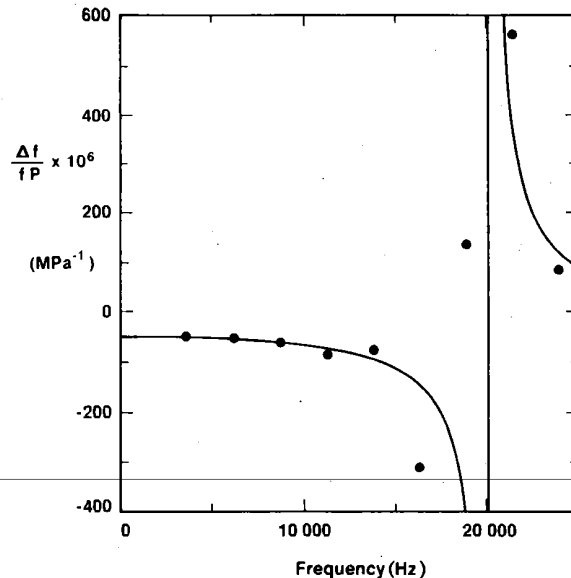

FIG. 11. Response of the shell to radially symmetric excitation as a function of frequency. The points are the average slopes of the curves in Fig. 9. The curve is calculated for an isotropic seamless shell using the theory of elasticity and the elastic constants tabulated for aluminum (see Table V). The idealized shell has a breathing resonance near 20.2 kHz.

(81) and (83)] and the value of A_1 obtained from other experiments. We shall see that most of the differences between this simple model and the data are attributable to the nonzero admittance of the 1.24-cm-thick aluminum shell.

The parameter $c_0/(V_0)^{1/3}$ is chosen to be 8135.350/s to best fit the first few $(0,s)$ modes. This value is used consistently throughout the remainder of this paper. For the $(0, s)$ modes, we have also included in the model some very small effects resulting from the vent hole and the transducer duct [Eqs. (59)–(64)]. These effects cannot be included for the $(1, s)$ modes because the orientations of the symmetry axes of the nearly degenerate submodes with respect to the vent and the duct have not been determined.

Figure 9 displays the deviations of all of the $(0, s)$ data from the model without shell-admittance effects. The nearly linear dependence of the deviations on pressure is exactly what one would expect for an admittance effect [Eq. (87)] because the speed of sound in argon at 296.31 K is a very weak function of pressure and the density of the argon is almost exactly proportional to pressure. The mode closest to the breathing resonance of the shell, the $(0,9)$ mode, shows the largest deviations (as much as 0.08% at 1 MPa). The $(0,9)$ data also depart from a linear pressure dependence.

Figure 10 displays the deviations of the frequency data for the $(1,2)$ and $(1,6)$ modes. The linear pressure dependence again demonstrates the effect of the shell admittance.

TABLE V. Properties of the aluminum shell.

$a = 0.063\ 493\ 2(1 - 4.7 \times 10^{-7} P^*)$ m
$h = 0.0124$ m
$\rho_{sh} = 2700$ kg/m³
$c_{sh} = 6420$ m/s
$\sigma = 0.355$

The data for other $(1,s)$ modes are similar.

In Fig. 11, we have plotted the average slopes of each of the deviation curves in Fig. 9. These slopes are compared with a calculation of the shell admittance based on elasticity theory [Eqs. (49)–(54)] and the properties of aluminum summarized in Table V. Thus the comparison is on an absolute basis. The slopes of the low-frequency (0,2), (0,3), and (0,4) modes lie very close to the calculated curve. The slopes for modes which are close to the calculated breathing resonance deviate substantially from the calculation. These are the same modes for which we measured very large excess half-widths.

Figures 7, 9, and 11, taken together, suggest that under radially symmetric excitation, the shell behaves like an oscillator with a resonance near 20.2 kHz, as predicted. However, this oscillator has large losses for which we have no quantitative model.

In Fig. 12, we have plotted the average slopes of the frequency deviations with pressure for each of the $(1,s)$ modes including those shown in Fig. 10. These slopes are also compared on an absolute basis with the calculation of the shell response given by Eq. (54) with numerical calculations of $S_1(k_{sh}a)$ as described in Ref. 18. Again, the agreement is quite good except very near the shell's resonance at 24.5 kHz. The data for the three (1,1) modes are shown in the inset along with a single point representing the (1,2) modes. The data are consistent with the extraordinarily large effect which an inertial reactance is expected to have on the lowest-frequency modes. The splitting of the three (1,1) modes may be related to asymmetric coupling to the Helmholtz resonance of the detector duct. Another possibility is asymmetric mechanical support of the resonator. A modified form of Eq. (57) which includes the effects of support stiffness can easily be derived.[19] The effective stiffness of the supports will differ for shell motion in the horizontal and vertical directions. Thus 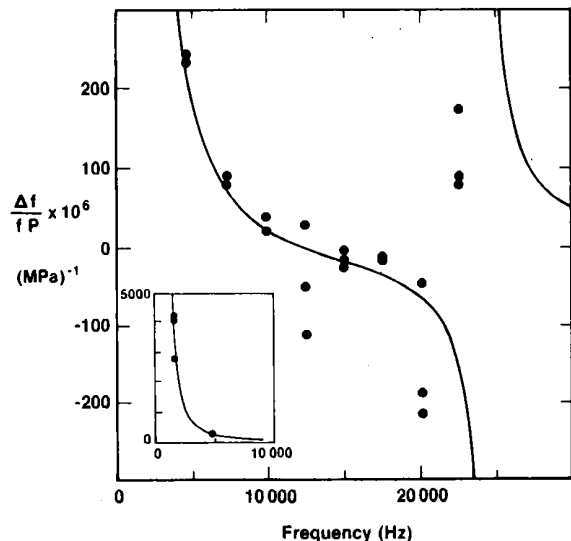the effects of support stiffness will differ for the various (1,1) modes, depending on the direction of the average gas motion. The data are consistent with a moderate stiffness effect which introduces some asymmetry; the major effect, however, is the inertial effect given by Eq. (57).

We carried out a few primitive experiments to directly measure the shell's resonances in air. A loudspeaker was used as a source and a phonograph needle in contact with the shell was used as a detector. The exact theory of elasticity predicts, for an aluminum, isotropic, spherical shell with the dimensions of our resonator, numerous resonances within the frequency range of our experiments. There are three degenerate resonances at zero frequency (and three more near 24.5 kHz), five degenerate resonances at 8.5 kHz, seven degenerate resonances at 11.2 kHz, nine degenerate resonances at 14.2 kHz, eleven degenerate resonances at 18.2 kHz, thirteen degenerate resonances at 23.0 kHz, and the nondegenerate breathing resonance at 20.2 kHz. Our crude experiments detected sharp resonances $(100 < Q < 1000)$ at 7.69, 8.07, 8.13, 8.50, 10.67, 10.72, 11.18, 13.80, 13.91, 13.97, 16.87, 17.39, 17.47, and 17.95 kHz. The loss factors $1/Q$ of these resonances are consistent with published data for losses in aluminum.[33,34] We would not expect to be able to detect all of the resonances with our relatively crude method of excitation and detection. We speculate that the observed resonances differ somewhat from the predicted ones because of the shell's asymmetric construction and method of support.

In these crude experiments, we did not detect the breathing resonance near the 20.2-kHz or the 24.5-kHz resonances. The large losses and frequency shifts near the breathing resonance that are evident in Figs. 7 and 9 have magnitudes that are roughly consistent with a value of Q_{sh} in Eq. (55) that is on the order of 10. If the breathing mode of the shell were really this lossy, it is plausible that we would not detect it in our crude experiment. We have, however, no explanation why the bending modes of the shell would have losses so much lower than those of the breathing mode.

FIG. 12. Elastic response of the shell to excitation with symmetry of $Y_{1m}(\theta,\phi)$ as a function of frequency. The points are the average slopes of curves such as those shown in Fig. 10. The curve is calculated for an isotropic, seamless shell using the theory of elasticity and the elastic constants tabulated for aluminum. The idealized shell has Y_{1m} resonances at 0 and 24.5 kHz.
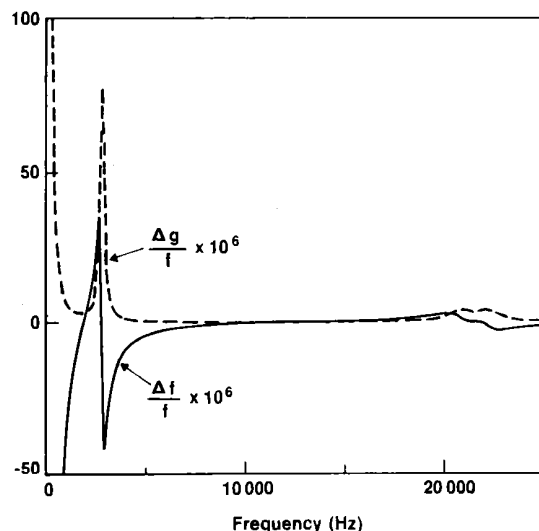

FIG. 13. Effects of the vent hole, the detector cavity, and the duct coupling the detector to the resonator's interior calculated using the model described in the text, for $P = 0.1$ MPa and $T = 296$ K.

269   J. Acoust. Soc. Am., Vol. 79, No. 2, February 1986

Moldover *et al.* : Spherical resonators   269

H. The vent hole and the duct

The shell admittance effects we have just considered vanish as the pressure is reduced. At low pressures, we expect that the effects of geometrical imperfections will remain. We shall now consider those which have an influence on our measurements.

In Fig. 13, we have displayed the calculated perturbations (for $P = 0.1$ MPa) to be added to f_N and g_N, resulting from the vent and the duct leading to the detector transducer [Eqs. (59)–(64)]. The duct is terminated by a cavity whose volume is 22 mm³. The vent is terminated by a radiation boundary condition.

The very large pertubation at the lowest frequencies is the result of the acoustic admittance of the open vent. This perturbation is most important for the (1,1) mode; however, the (1,1) mode interacts so strongly with the shell motion that we had no chance of detecting the much smaller vent and duct perturbation. The Helmholtz resonance near 3 kHz is also prominent in Fig. 13. We have commented that its effect on excess half-width may have been seen. Its effect on the frequency is also noticeable and has been included in Figs. 15 and 17 below. The small peaks in Δg near 21 kHz are associated with the organ pipe resonances of the duct and vent. They fall between the (1,8) and the (0,9) modes of the gas in the spherical shell. As the pressure is raised, the peaks in Δg become larger and narrower and they shift towards higher frequencies; however, if our model is roughly correct, these peaks are never big enough to explain the differences between the data for the (0,9) mode and theory.

In Fig. 14, we provide a striking experimental test of these perturbation calculations using data from an earlier configuration of the same resonator. The half-widths of the (0,s) resonances were measured at 0.1 MPa before and after drilling an extra, oversized vent hole through the shell. This 0.16-cm-diam vent produced a large increase in $g_{0.5}$; however it did not noticeably affect the half-widths of the other (0,s) modes. This is exactly the expected result because this 0.62-cm-long vent happens to be resonant (as an open organ pipe) at the same frequency as the (0,5) mode.
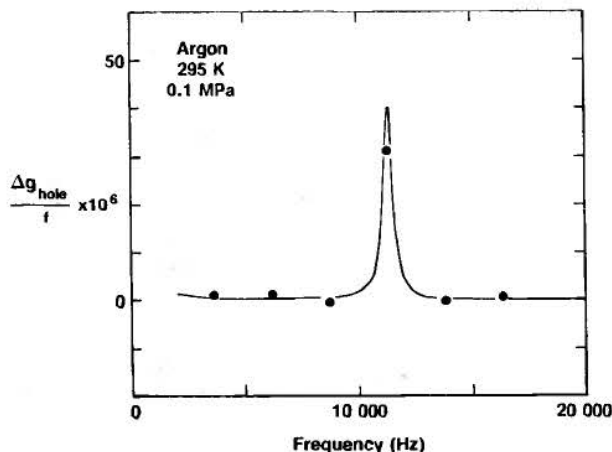
I. The Importance of the nondegenerate modes

We now illustrate the importance of the nondegenerate modes for making accurate measurements. We shall extrapolate the (0,s) and (1,s) frequencies to zero pressure. The nondegenerate (0,s) frequencies show two orders of magnitude greater consistency than the resolved, nearly degenerate (1,s) frequencies.

In Fig. 15, we display the results of extrapolating the (0,s) frequencies to zero pressure after accounting for the viscothermal boundary layer. Separate calculations show the effects of including and omitting the vent and the duct perturbations. It is remarkable that the extrapolations for the six modes (0,3) through (0,8) have an average of $(1.4 \pm 1.8) \times 10^{-6}$ when the effects of the duct and the vent are ignored. (The quoted error is the rms deviation from the mean.) This extraordinarily high degree of internal consistency is a clear illustration of the fact that these resonances are not affected by the shape perturbations which we know are about 300 parts in 10^6.

Figure 15 also shows that the duct perturbs the (0,2) mode by a relatively large amount which is not satisfactorily predicted by our model. For this reason, the (0,2) mode was omitted from the averages quoted above. For the six modes (0,3) through (0,8), the effects of including the vent and duct perturbations changes the average to $(1.5 \pm 2.2) \times 10^{-6}$.

Our criterion for choice of the parameter $c_0/(V_0)^{1/3}$ was the requirement that the average extrapolated $\Delta f/f$ for the first seven (0,s) modes be near zero. The scatter in these seven points in Fig. 15 is not instrumental noise. If the measurements were repeated, the same results would occur. Thus one can also say that these zero-pressure frequencies are inconsistent with each other and that 2 parts in 10^6 is the approximate size of the rms inconsistency in $\Delta f/f$. The
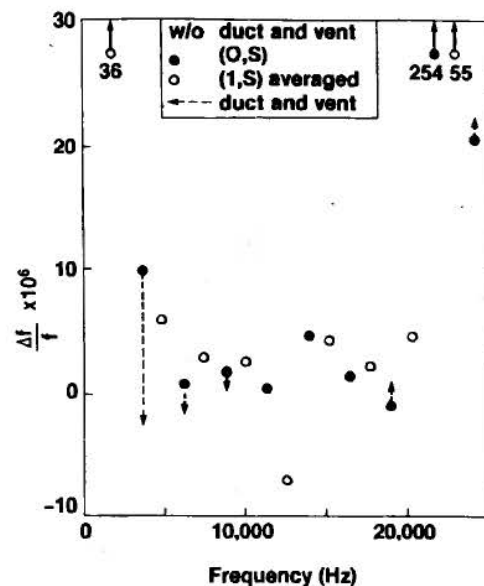
FIG. 15. Measured zero-pressure frequencies minus calculated frequencies for the (0,s) (solid symbols) and (1,s) (open symbols) modes. The symbols represent the zero pressure intercepts of straight lines fitted to data such as those in Figs. 9 and 10. The intercept for the (0,9) mode at 21.4 kHz is 254 parts in 10^6 above the predicted value. The (0,9) mode is close to the resonances in the vent hole and coupling duct.

FIG. 14. Excess half-width resulting from drilling an oversized (0.16-cm-diam and 1.27-cm-long) vent hold through the shell.

large $\Delta f / f$ for the (0,9) mode may mean that the data do not reach low enough pressures to ignore the breathing resonance of the shell.

In Fig. 16, we display the results of extrapolating the (1,s) frequencies to zero pressure after accounting for the viscothermal boundary layer. The extrapolated frequencies span a range of 500 parts in 10^6 about the frequencies that would be expected for a perfectly spherical resonator. The curves in Fig. 16 represent Eqs. (68)–(69). The two parameters in these equations (ϵ_0 and ϵ_1) characterizing deviations from sphericity were fit to the data shown. Their values are reasonable in light of the known machining tolerances.

For each triply-degenerate (1,s) mode, the lowest order of boundary shape perturbation theory[24] predicts that the average of the three components' zero-pressure frequencies is equal to the zero-pressure frequency for a geometrically perfect spherical resonator. We have computed these averages for the seven (1,s) modes from (1,2) through (1,8) and compared them with the frequencies predicted by our model. The zero-pressure frequencies differ from our model by $(5.2 \pm 1.8) \times 10^{-6}$. Thus the (0,s) and (1,s) families of modes differ by only $(3.8 \pm 2.5) \times 10^{-6}$.

From this discussion, the experimentalist is forced to conclude that if he wishes to make really accurate speed of sound measurements with a resonator, he has two options: (1) use the nondegenerate, radially symmetric modes, or (2) measure the frequency of each of the components of a degenerate mode and use their average. Obviously the first option is less demanding.

III. THEORY AND EXPERIMENT: A FINAL COMPARISON

Up to this point, the comparison of experiment and theory has been structured to test or illustrate particular aspects
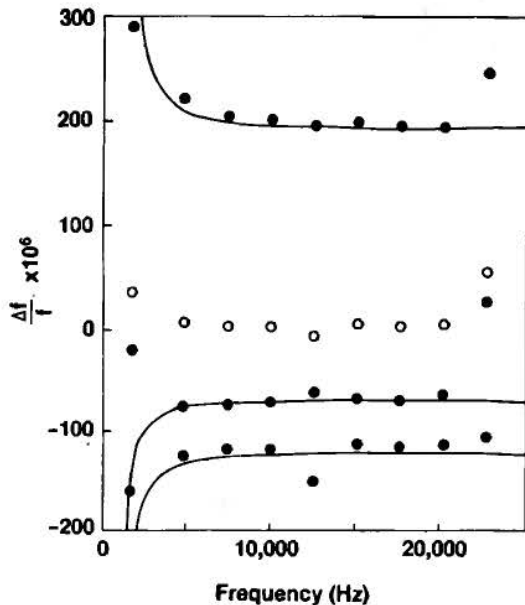

FIG. 16. Measured zero-pressure frequencies minus calculated frequencies for the (1,s) modes. The solid symbols represent the zero pressure intercepts of straight lines fitted to data such as those displayed in Fig. 10. The curves are obtained from Eqs. (68) and (69) with the parameters $\epsilon_0 = 3.5 \times 10^{-4}$ and $\epsilon_1 = 3.1 \times 10^{-4}$. The open symbols are averages of the three zero-pressure frequencies for each (1,s) set of modes. These averages are also plotted in Fig. 15.
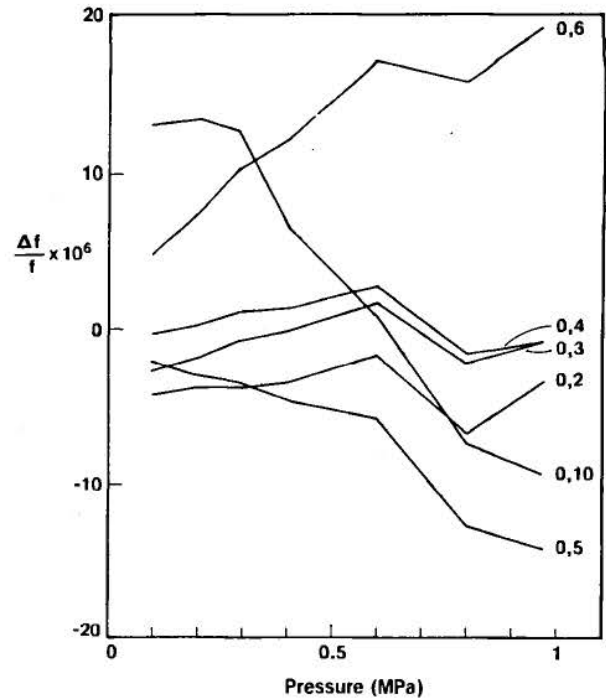

FIG. 17. Measured frequencies minus calculated frequencies for six of the (0,s) modes as functions of pressure. The calculation includes the effects of the thermal boundary layer, the holes in the shell, and the dynamic response of the shell.

of the theory. Now we include all aspects at once to indicate the extent to which experiment and theory agree.

In Fig. 17, we plot the differences between the frequencies measured for the (0,s) modes and our most complete model. This model includes the viscothermal boundary layer [Eqs. (81) and (83)], shell elasticity [Eqs. (49)–(54) and Table V], the pressure dependence of the speed of sound and the transport properties (Table III), the perturbations from the vent and duct, and a small pressure dependence of the shell's radius resulting from hydrostatic compression.

Figure 17 shows that all the data for 6 of the 9 (0,s) modes we studied fall within ± 18 parts in 10^6 of this model in the range 0.1–1.0 MPa. Most of the data for the (0,7), (0,8), and (0,9) modes fall off this plot. This strongly suggests that the admittance of the prototype resonator near its breathing mode is poorly modeled.

IV. ANTICIPATED IMPROVEMENTS

We are now constructing a spherical resonator out of stainless steel. The higher density of steel will lead to perturbations due to shell elasticity which are a factor of three smaller at low frequencies. The hemispheres have been welded together. We hope this will reduce losses associated with the shell's motion still further. The breathing frequency will not be very different. Both the source and the detector transducers will be high-impedance devices mounted flush with the interior surface of the shell. This will eliminate the duct and its associated Helmholtz resonance. Finally, during measurements of the gas resonances, the vent will be plugged. We anticipate that reducing these perturbations will further improve the agreement between theory and experiment.

ACKNOWLEDGMENT

[1] M. R. Moldover and J. B. Mehl, in *Precision Measurements and Fundamental Constants II*, edited by B. N. Taylor and W. D. Phillips (Natl. Bur. Stand., Washington, DC, 1984), Spec. Publ. 617, pp. 281–286.

[2] J. B. Mehl and M. R. Moldover, J. Chem. Phys. **74**, 4062–4077 (1981).

[3] J. B. Mehl and M. R. Moldover, in *Proceedings of the Eighth Symposium on Thermophysical Properties*, edited by J. V. Sengers (Am. Soc. Mech. Eng., New York, 1982), pp. 134–141.

[4] C. M. Knobler, Pure Appl. Chem. **55**, 455–466 (1983).

[5] J. P. M. Trusler, Ph. D. thesis, University College, London, 1984.

[6] R. Keolian, S. Garrett, J. Maynard, and I. Rudnick, J. Acoust. Soc. Am. Suppl. 1 **64**, S561 (1973); and Bull. Am. Phys. Soc. **24**, 623 (1979).

[7] J. S. Brooks and R. B. Hallock, Rev. Sci. Instrum. **54**, 1199–1201 (1983).

[8] P. Hess, in *Topics in Current Chemistry* (Springer, Berlin, 1983), Vol. III, pp. 1–32.

[9] We define the Q as the resonance frequency divided by the full resonance width at $1/\sqrt{2}$ of the maximum amplitude.

[10] M. Greenspan, in *Physical Acoustics* (Academic, New York, 1965), Vol. IIA, pp. 1–45.

[11] M. B. Ewing, M. L. McGlashan, and J. P. M. Trusler, *Metrologia* (to be published).

[12] J. B. Mehl and M. R. Moldover, J. Chem. Phys. **77**, 455–465 (1982).

[13] G. Kirchhoff, Ann. Phys. Chem. (Fifth Ser.) **134**, 177–193 (1868); English translation by R. B. Lindsay in *Benchmark Papers in Acoustics: Physical Acoustics*, edited by R. B. Lindsay (Dowden, Hutchinson, & Ross, Stroudsburg, PA, 1974), pp. 7–19.

[14] J. W. S. Rayleigh, *Theory of Sound*, 2nd ed., 1896 (reprinted by Dover, New York, 1945), Sec. 348.

[15] P. M. Morse and K. U. Ingard, *Theoretical Acoustics* (McGraw-Hill, New York, 1968), Eqs. (6.4.22). Elimination of p from the first and second of these equations gives our Eq. (8).

[16] P. M. Morse and H. Feshbach, *Methods of Theoretical Physics* (McGraw-Hill, New York, 1953), Chap. 13, Eq. 13.1.6.

[17] K. F. Herzfeld, Phys. Rev. **53**, 899–906 (1938).

[18] M. Greenspan, unpublished notes on the spherical acoustic resonator.

[19] J. B. Mehl, J. Acoust. Soc. Am. **78**, 782–788 (1985).

[20] See also Ref. 14, Sec. 350; and Ref. 15, Secs. 6.4 and 9.1.

[21] Reference 15, Sec. 9.4.

[22] Reference 16, pp. 1052–1055.

[23] J. B. Mehl, J. Acoust. Soc. Am. **71**, 1109–1113 (1982).

[24] J. B. Mehl, J. Acoust. Soc. Am. **79**, 278–285 (1986).

[25] M. R. Moldover, M. Waxman, and M. Greenspan, High Temp. High Pressure **11**, 75–86 (1979).

[26] J. Kestin, S. T. Ro, and W. A. Wakeham, J. Chem. Phys. **56**, 4119–4124 (1972).

[27] J. J. deGroot, J. Kestin, H. Sookiazian, and W. A. Wakeham, Physica **92A**, 117–144 (1978).

[28] J. M. H. Levelt Sengers, M. Klein, and J. S. Gallagher, in *American Institute of Physics Handbook*, edited by D. E. Gray (McGraw-Hill, New York, 1972), pp. 4–219.

[29] J. S. Gallagher and M. Klein, J. Res. Natl. Bur. Stand. **75A**, 337–385 (1971).

[30] A. S. El-Hakeem, J. Chem. Phys. **42**, 3132 (1963).

[31] Reference 14, Sec. 331.

[32] J. B. Mehl, J. Acoust. Soc. Am. **64**, 1523–1525 (1978).

[33] W. P. Mason, *Piezoelectric Crystals and Their Applications in Ultrasonics* (Van Nostrand, New York, 1950), p. 420.

[34] L. Cremer, M. Heckl, and E. Ungar, *Structure-Borne Sound* (Springer, New York, 1973), Tables III.1 and III.2.